Shackleton, N.J., Curry, W.B., Richter, C., and Bralower, T.J. (Eds.), 1997
Proceedings of the Ocean Drilling Program, Scientific Results, Vol. 154

36. INORGANIC GEOCHEMICAL COMPOSITION OF OLIGOCENE TO MIOCENE SEDIMENTS AND PRODUCTIVITY VARIATIONS IN THE WESTERN EQUATORIAL ATLANTIC: RESULTS FROM SITES 926 AND 929[1]

G.P. Weedon[2] and N.J. Shackleton[3]

ABSTRACT

Approximately 500 closely spaced pelagic sediment samples, representing the latest Miocene, middle Miocene, Oligocene/Miocene boundary, and mid-Oligocene, were obtained from two sites on the Ceara Rise. Inductively coupled plasma emission spectroscopy was used to measure the concentrations of Al, Ca, P, K, Si, Ti, Ba, V, and Cu. Normalization by Al was used to allow for variable carbonate dilution of the siliciclastic components. For comparison, Holocene hemipelagic silty clay samples from the Amazon Fan were also analyzed. The elemental ratios were used to infer varying sediment compositions and surface productivity.

On average, K/Al and Ti/Al values are similar in the latest Miocene to Holocene values, but are lower in all the older samples. This reflects the switch from kaolinite to illite-dominated clay minerals in the late Miocene, during the growth of the Amazon Fan. Average Ba/Al, P/Al, and Si/Al values from the mid-Oligocene and Oligocene/Miocene boundary samples are higher than those of the middle Miocene to Holocene samples. The higher ratios suggest phases of relatively high surface productivity, which at least partly accounts for the occurrence of biosiliceous plankton microfossils in these intervals.

In the mid-Oligocene and Oligocene/Miocene boundary samples, variations in Ba/Al, P/Al, and Si/Al are correlated, suggesting variable productivity over short time periods. Maximum productivity occurred during times of maximum burial/preservation of calcium carbonate. Spectral analysis reveals statistically significant regular cyclicity in all of these parameters from these intervals. The cyclicity is associated with the 40,000-yr obliquity orbital-climatic cycles. The dominance of this cyclicity, and lack of evidence for 20,000-yr cycles, suggests that short-term variations in productivity were driven by high-latitude climatic processes perhaps acting through bottom-water production.

INTRODUCTION

Drilling at five sites on the Ceara Rise during Ocean Drilling Program (ODP) Leg 154 provided a nearly complete record, at the tens of thousands of years scale, of pelagic sedimentation since the mid-Paleocene (Fig. 1; Curry, Shackleton, Richter, et al., 1995). The cores were collected from a depth transect of 1.5 km to investigate the paleoceanographic and paleoclimatic history of the equatorial Atlantic and South America. This study attempts to characterize the variations in the composition of the sediments by using inorganic elemental ratios. Four time intervals have been selected for sampling from cores from a relatively shallow site on the Rise, Site 926 (currently at a water depth of 3600 m). Additionally, samples have been obtained for the oldest time period at the deepest site (Site 929 at 4360 m water depth). The samples have been analyzed for a suite of elements using inductively coupled plasma-atomic emission spectroscopy (ICP-AES).

Individual 10-cm^3 samples were collected at 10-cm intervals. The time intervals represented by the samples are the latest Miocene, the middle Miocene, the Oligocene/Miocene boundary and the late early Oligocene to early late Oligocene (henceforth described as "mid-Oligocene;" Table 1). Sediment compositional variations have been monitored through normalization of elemental concentrations by aluminum. This method permits the examination of changing siliciclastic mineralogy and surface productivity, although the interpretations of particular elemental ratios is not always straightforward. The sampling strategy has allowed the study of variations in these factors over time scales of both tens of millions of years and tens of thousands of years.

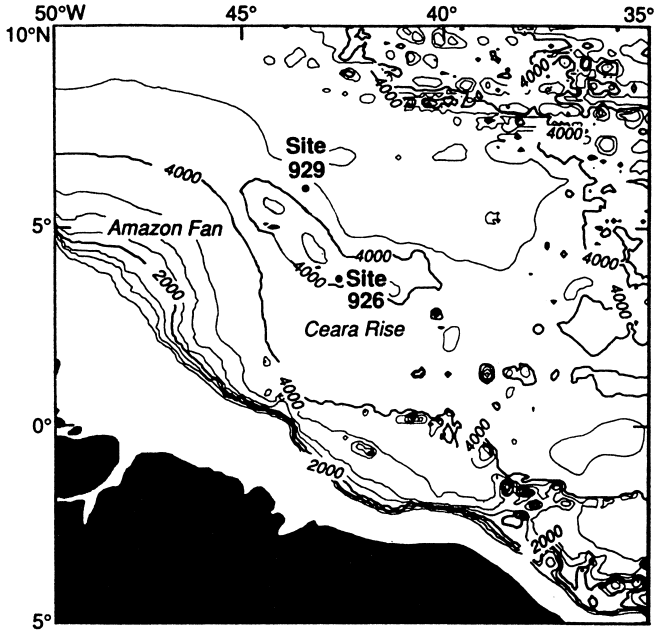

Figure 1. Location of the sites on the Ceara Rise used for sampling.

Since the mid-Oligocene, there have been major paleogeographical changes in the western equatorial Atlantic. In particular, the Ceara Rise has subsided as the Atlantic widened from about 6150 to 6470

[1]Shackleton, N.J., Curry, W.B., Richter, C., and Bralower, T.J. (Eds.), 1997. *Proc. ODP, Sci. Results,* 154: College Station, TX (Ocean Drilling Program).

[2]Department of Geology, University of Luton, Park Square, Luton, Bedfordshire LU1 3JU, United Kingdom. graham.weedon@luton.ac.uk

[3]Godwin Laboratory, Department of Earth Sciences, University of Cambridge, Free School Lane, Cambridge, Cambridgeshire, United Kingdom.

Table 1. Locations of the samples analyzed for elemental concentrations.

Age	Biozone	Core, section, interval (cm)	Depth (mbsf)	Composite depth (mcd)
Amazon Fan Samples				
Holocene	CN15/N23	155-942C-2H-6, 140–145	13.23	
		155-942C-2H-7, 10–14	13.42	
		155-942C-2H-7, 30–35	13.63	
Ceara Rise Samples				
latest Miocene	CN9b/N17	Top: 154-926B-17H-2, 54–56	151.55	171.02
		Base: 154-926B-17H-4, 104–106	155.05	174.62
latest Miocene	CN9b/N17	Top: 154-926C-17H-6, 107–109	161.08	180.81
		Base: 154-926C-17H-6, 147–149	161.48	181.21
latest Miocene	CN9b/N17	Top: 154-926B-18H-2, 74–76	161.25	181.29
		Base: 154-926B-18H-2, 94–96	161.45	181.49
latest Miocene	CN6/N14	Top: 154-926B-25H-6, 54–56	226.05	252.06
		Base: 154-926B-25H-1, 144–146	226.95	252.96
latest Miocene	CN5/N12-13	Top: 154-926A-26H-1, 44–46	232.45	260.81
		Base: 154-926A-26H-4, 144–146	237.95	266.31
Miocene/Oligocene	CN1/P22-N4	Top: 154-926B-50X-1, 14–16	461.55	491.36
		Base: 154-926B-50X-CC, 44–46	470.75	500.56
latest Oligocene	CN1/P22	Top: 154-926B-51X-1 14–16	471.15	500.96
		Base: 154-926B-51X-CC, 34–36	480.75	510.56
late Oligocene	CP19a/P21a	Top: 154-926B-64X-1, 4–6	596.65	626.36
		Base: 154-926B-64X-CC, 24–26	606.05	635.96
early Oligocene	CP18/P19-20	Top: 154-929A-47X-1, 0–2	436.11	451.53
		Base: 154-929A-47X-CC, 30–32	445.81	461.23

Note: All the Ceara Rise samples were collected in continuous runs at 10-cm intervals. Nannofossil and planktonic foraminifer biozone designations are also provided.

km along the line of the equator (Smith et al., 1994). Sea level has varied substantially (Haq et al., 1987) and the carbonate compensation depth has changed, whereas the extensive Miocene epeiric seas of South America were replaced by terrestrial conditions. The growth of the Amazon Fan in the latest Miocene was perhaps associated with rapid uplift of the Andes (Castro et al., 1978; Benjamin et al., 1987; Rasanen et al., 1995; Webb, 1995). All these events may have affected the sediment compositions examined here.

ANALYTICAL METHODS

The elemental concentrations of Al, Ba, Ca, Cu, K, P, Si, Ti, and V were determined using a Perkin Elmer Plasma 40 ICP-AES. About 5 g of sediment was crushed using a pestle and mortar and then air-dried at 105°C. Lithium metaborate (1.25 g) was mixed with 0.25 g of sample powder in a graphite crucible and placed in a muffle furnace at 1050°C for 20 min. The melt was tipped into 3.5% nitric acid and mixed until complete dissolution had occurred (after 30 min to 1 hr). The solution was filtered to remove any carbon particles from the crucible and made up to 250 µL with distilled water. Calibration was based on four international rock standards (CANMET LKSD1 through 4). Background correction was applied during analysis to minimize potential matrix effects. A monitor solution was run after every six unknown solutions to allow correction for drift. Accuracy and precision is presented for each element in Table 2. The results are expressed as elemental (not oxide) concentrations in percentages for the major elements and in micrograms per gram, or parts per million, for the minors (Table 3). Copper and vanadium values were detectable, but below the limits of quantitation (i.e., ten times the standard deviation of the blank: 100 µg/g for Cu and 250 µg/g for V) in virtually all samples. Because these elements were detectable, but not accurately quantifiable, the results for Cu and V are presented in Table 3, but have not been illustrated. A correlation matrix for the elemental concentrations is presented in Table 4.

Calcium carbonate determinations were performed on splits of 37 samples from Core 154-926B-17H at the University of Stockholm by J. Backman. A 30-mg sample was dried and crushed using a Retch mill grinder. Analysis was performed using a UIC CO_2 coulometer and the results are listed in Table 5.

ELEMENTAL RATIOS AS MONITORS OF SEDIMENT COMPOSITION AND ENVIRONMENTAL PARAMETERS

The pelagic sediments of the Ceara Rise consist of nannofossil oozes and chalks that alternate, on a decimeter-to-meter scale, with clayey nannofossil oozes and chalks. The causes of these variations in carbonate contents are unclear, but are at least partly related to carbonate dissolution as revealed by foraminifer preservation (Pearson et al., this volume). Whatever processes were responsible for the carbonate fluctuations, their regularity is diagnostic of indirect control by orbital-climatic cycles (Weedon, et al., this volume).

To allow for the substantial variations in carbonate content, normalization of the element concentrations by aluminum has been employed (Shimmield and Mowbray, 1991; Norry et al., 1994). This procedure relies on the presence of aluminum in the non-carbonate (principally clay mineral) fraction. Although it is not suggested that the average content of aluminum in the non-carbonate fraction was constant, it can reasonably be assumed that it varied by a much smaller factor than bulk carbonate contents. Support for the assertion that aluminum is associated with the siliciclastic fraction of these sediments comes from the very high correlation (Table 4) with Si, Ti, and K and the inverse correlation with Ca as illustrated in Fig. 2.

Since the composition of the siliciclastic fraction of the sediments is the main subject of this study, samples were analyzed from the Holocene Amazon Fan. The Amazon Fan is not active during the current sea level high-stand. Therefore, three samples that date from the last glacial maximum were obtained from hemipelagic silty clay on a channel levee from Site 942, ODP Leg 155 (Flood, Piper, Klaus, et al., 1995). The current water depth of this site is 3350 m so it would have been very close to the carbonate compensation depth at 18 ka. The Ceara Rise and Amazon Fan currently underlie a low productivity zone; the fan samples provide an indication of near-Holocene fine-grained siliciclastic sediment compositions (Table 3).

Table 2. Accuracy and precision based on replicate analyses of CANMET lake sediment standard LKSD 4.

Element	No. repeat analyses	Mean of analyses	SD	LKSD 4	Accuracy (%)	Precision (%)
Al	20	6.46%	0.136%	6.40%	100.9	2.1
Ca	20	2.89%	0.069%	2.86%	101.3	2.4
P	20	0.088%	0.0028%	0.087%	100.7	3.2
K	20	1.36%	0.064%	1.33%	102.4	4.7
Si	20	27.5%	0.74%	27.5%	100.0	2.7
Ti	20	0.487%	0.011%	0.480%	101.4	2.2
Ba	20	2018 µg/g	65 µg/g	2000 µg/g	100.9	3.2
V	6	106 µg/g	10 µg/g	106 µg/g	100.0	9.4
Cu	19	63 µg/g	7 µg/g	65 µg/g	96.9	11.1

Notes: Accuracy is defined as 100% times the mean of the repeat analyses divided by the expected value. Precision is defined as 100% times the best estimate standard deviation (σ_{n-1}) divided by the mean of the repeats. SD = standard deviation.

The elements chosen for study are inferred to act, once normalized by aluminum, as proxies for sediment composition and paleoceanographic parameters following the strategy of, for example, Shimmield and Mowbray (1991). Many factors can influence elemental ratios, so each element is considered in turn.

In pelagic sediments, potassium resides almost exclusively in clay minerals and in particular within illite (Van Buchem et al., 1994). Absolute potassium concentrations are strongly correlated with Al and Ti (Table 4; Fig. 2). Titanium resides within heavy minerals such as ilmenite and rutile and within clay minerals. Consequently, the Ti/Al ratio provides an indication of the relative proportions of heavy minerals in the siliciclastic fraction and variations in clay mineralogy (Schmitz, 1989; Shimmield and Mowbray, 1991). The association of Ti with the siliciclastic components explains the high correlation with Al, Si, and K, and the inverse correlation with Ca in Table 4.

Barium is deposited in pelagic sediments as biogenic barites, and is incorporated structurally within biogenic calcite and in clay minerals (Dymond et al., 1992; Lea and Spero, 1994; Gingele and Dahmke, 1994). Consequently, high barium concentrations can follow other productivity proxies. As an example, Ba/Al values from recent sediments were used to monitor productivity variations over tens of thousands of years off the coast of Oman (Shimmield and Mowbray, 1991; Weedon and Shimmield, 1991). Since barium occurs in siliciclastic minerals, however, an estimation of detrital Ba/Al values is needed. In the three Amazon Fan samples analyzed, the ratios ranged from 0.0032 to 0.0034, whereas average values for siliciclastic minerals are 0.005 to 0.01 (Dymond et al., 1992). Sulfate reduction can cause barite dissolution (Brumsack and Gieskes, 1983). At Sites 926 and 929, pore-water sulfate concentrations are moderately reduced compared to seawater (Curry, Shackleton, Richter, et al., 1995). Because some sulfate reduction has occurred in Ceara Rise sediments, the Ba/Al ratios measured may have been lowered during diagenesis. Therefore, in this study, values that are higher than detrital values (i.e., above 0.01) have been taken as indicative of enhanced productivity. Using all the samples examined here, Ba concentrations are weakly negatively correlated with the siliciclastic elements Al, K, and Ti (Table 4). This inverse relationship suggests that, on average, most Ba in Ceara Rise sediments is not associated with clays

As phosphorus is a limiting nutrient in the oceans and is associated with organic matter, phosphorus concentrations in sediments have been used to monitor changing surface productivity (Filippelli and Delaney, 1994). Pauses in sedimentation and hiatuses can lead to phosphorus remobilization and authigenic concentration at discrete horizons. However, at Site 926, sedimentation rates were relatively high and there is no evidence of hiatuses (Curry, Shackleton, Richter, et al., 1995). Similarly, dysoxic and anoxic bottom waters can lead to increased recycling of phosphorus into the water column, which decreases the proportion buried (Van Cappellen and Ingall, 1994). Yet on the Ceara Rise, there is no evidence for laminated sediments; all of the pelagic sediments are thoroughly bioturbated, and the organic carbon concentrations are consistently very low (<0.25%; Curry, Shackleton, Richter, et al., 1995). Some P is incorporated in detrital minerals, and here it is weakly positively correlated with Al, Si, Ti, and K (Table 4). Hence, as for barium, a comparison with the Holocene Amazon Fan samples has been used to assess whether particular values indicate enhanced productivity

Silicon is strongly correlated with the siliciclastic elements Al, Ti, and K, reflecting its presence in clay minerals and, probably minor, quartz. Potentially, though, the Si/Al value could depend partly on concentrations of biogenic opal (Lyle et al., 1988; Charles et al., 1991). Indeed, diatoms and radiolaria were observed forming significant proportions of the lower Miocene and lower Oligocene sediment, although no chert was encountered (Curry, Shackleton, Richter, et al., 1995). Although the occurrence of biogenic silica can be indicative of high productivity, the factors that control the concentrations in ancient sediments are complex (Archer et al., 1993). For example, silica dissolution in carbonate-rich sediments during burial is a function of absolute silica concentrations. Therefore, in the case of sediments that received a constant flux of biogenic silica, but variable carbonate, Si/Al ratios, or silica expressed on a carbonate-free basis, would yield a spurious variation related to the effect of carbonate concentration upon silica dissolution (Archer et al., 1993). This would produce a covariation of carbonate and Si/Al values. In such situations other proxies such as Ba/Al and P/Al are needed to check that the Si/Al variations include a productivity component.

Vanadium has been observed at a concentration well above that of "average shale" in strata associated with reduced bottom-water oxygenation and under areas of high productivity (Brumsack, 1986; Arthur et al., 1989). Elevated V deposition appears to be associated with binding to organic matter. However, in all the samples analyzed, vanadium occurs at levels below the limit of quantitation. Copper is also associated with sediments containing high organic carbon concentrations associated with areas of high productivity (Arthur et al., 1989). As for vanadium, concentrations are always below the limit of quantitation. For both of these elements, the low concentrations are probably connected to the very low total organic carbon contents in the cores examined, caused by thorough ventilation during bioturbation. The V and Cu concentrations are recorded in Table 3, but since these elements occur in detectable, but not accurately quantifiable levels, they are not illustrated and are not discussed further.

Part of the scatter observed in the plot of Ca vs. Al for all samples (Fig. 2) might reflect the presence of calcium within clays and long term changes in clay mineralogy. However, there is evidence for a linear relationship between Ca/Al and carbonate divided by non-carbonate in Core 154-926B-17H, and when plotted stratigraphically, this ratio covaries with $\%CaCO_3$ (Fig. 3). Hence, we have used plots of Ca/Al as indicative of carbonate contents over short stratigraphic intervals.

RESULTS

Long-Term Changes in Elemental Ratios

To gauge the long-term changes in the elemental ratios, all of the results are plotted for Site 926 in Figure 4. For comparison, the vertical dashed lines indicate the ratios determined for the Holocene Amazon Fan samples.

The estimated average carbonate contents since the mid-Oligocene show small changes over millions of years in terms of variance and average values. This may be partly related to changing dissolution on the seafloor associated with the depth of the lysocline and/or to changing dilution by the siliciclastic flux. Average barium ratios in the latest Miocene and middle Miocene are essentially identical to the Holocene Amazon Fan hemipelagic silty clay. At the Oligocene/Miocene boundary and in the mid-Oligocene, the ratios are considerably higher, probably because of much higher productivity. This is confirmed by the very similar pattern found for phosphorus

Table 3. Elemental concentrations for samples from the Ceara Rise and Amazon Fan.

Core, section, interval (cm)	Depth (mbsf)	Depth (mcd)	Al (%)	Ca (%)	P (%)	K (%)	Si (%)	Ti (%)	Ba (ppm)	V (ppm)	Cu (ppm)
155-942C-											
2H-6, 140–145	13.23	13.23	10.48	1.81	0.059	2.40	23.6	0.561	431	151	56
2H-7, 10–14	13.42	13.42	10.13	1.29	0.062	2.44	24.5	0.583	439	148	40
2H-7, 30–35	13.63	13.63	9.84	2.25	0.098	2.24	22.4	0.551	400	151	57
154-926B-											
17H-2, 54–56	151.55	171.02	2.39	21.29	0.028	0.59	5.1	0.132	185	105	23
17H-2, 64–66	151.65	171.12	2.34	14.97	0.026	0.69	5.6	0.157	146	20	23
17H-2, 74–76	151.75	171.22	4.90	17.83	0.036	1.30	10.8	0.277	297	149	37
17H-2, 84–86	151.85	171.32	5.28	16.34	0.034	1.21	11.2	0.307	294	132	33
17H-2, 94–96	151.95	171.42	5.26	16.84	0.035	1.33	11.3	0.297	278	118	12
17H-2, 104–106	152.05	171.52	3.26	20.54	0.025	0.74	6.8	0.176	196	83	59
17H-2, 114–116	152.15	171.62	3.93	19.29	0.035	0.95	8.3	0.212	215	113	37
17H-2, 124–126	152.25	171.72	4.05	16.85	0.026	0.98	8.5	0.219	194	81	37
17H-2, 134–136	152.35	171.82	5.66	23.81	0.034	1.04	11.0	0.285	143	40	26
17H-2, 144–146	152.45	171.92	3.81	23.81	0.029	1.47	7.6	0.250	188	57	26
17H-3, 4–6	152.55	172.02	2.87	19.96	0.026	0.85	5.8	0.146	159	49	19
17H-3, 14–16	152.65	172.12	3.12	20.30	0.035	0.78	6.8	0.179	212	80	6
17H-3, 24–26	152.75	172.22	3.75	20.10	0.036	0.99	8.6	0.200	218	79	18
17H-3, 34–36	152.85	172.32	4.88	16.22	0.032	1.27	11.0	0.274	252	76	7
17H-3, 44–46	152.95	172.42	5.17	16.30	0.030	1.14	11.0	0.224	245	89	16
17H-3, 54–56	153.05	172.52	4.29	18.79	0.032	1.16	9.3	0.242	239	21	16
17H-3, 64–66	153.15	172.62	3.64	20.24	0.030	0.95	7.8	0.194	203	64	13
17H-3, 74–76	153.25	172.72	3.26	20.67	0.032	0.82	7.3	0.174	172	69	14
17H-3, 84–86	153.35	172.82	3.56	20.98	0.043	0.64	7.3	0.176	172	57	27
17H-3, 94–96	153.45	172.92	2.97	21.53	0.025	0.78	6.3	0.190	213	64	14
17H-3, 104–106	153.55	173.02	3.01	22.45	0.029	1.22	7.0	0.198	148	57	23
17H-3, 114–116	153.65	173.12	3.99	18.65	0.030	1.45	8.5	0.199	185	69	38
17H-3, 124–126	153.75	173.22	4.47	19.15	0.028	0.96	9.2	0.159	199	36	27
17H-3, 134–136	153.85	173.32	5.66	17.49	0.039	0.83	11.3	0.134	248	83	24
17H-3, 144–146	153.95	173.42	4.17	19.28	0.032	1.09	8.3	0.169	200	63	31
17H-4, 4–6	154.05	173.52	5.26	15.71	0.039	1.71	11.3	0.269	234	88	65
17H-4, 14–16	154.15	173.62	3.58	20.31	0.033	0.97	7.8	0.199	183	14	36
17H-4, 24–26	154.25	173.72	2.65	18.99	0.024	0.80	5.6	0.135	139	27	26
17H-4, 34–36	154.35	173.82	3.99	17.81	0.032	1.16	8.7	0.214	193	43	33
17H-4, 44–46	154.45	173.92	6.05	14.97	0.031	1.44	13.1	0.290	271	73	24
17H-4, 54–56	154.55	174.02	6.77	13.72	0.042	1.79	14.3	0.360	278	72	26
17H-4, 64–66	154.65	174.12	6.47	13.98	0.036	1.51	13.5	0.333	279	65	23
17H-4, 74–76	154.75	174.22	4.65	16.85	0.028	1.40	9.7	0.243	215	99	30
17H-4, 84–86	154.85	174.32	4.77	16.56	0.034	1.38	9.6	0.239	221	77	26
17H-4, 94–96	154.95	174.42	4.98	15.32	0.036	1.49	10.3	0.249	208	68	28
17H-4, 104–106	155.05	174.52	5.51	14.60	0.033	1.58	11.3	0.278	223	108	30
17H-4, 114–116	155.15	174.62	3.43	17.85	0.031	1.01	6.9	0.171	153	74	26
154-926C-											
17H-6, 107–109	161.08	180.81	3.34	18.59	0.040	0.79	6.9	0.164	179	81	25
17H-6, 117–119	161.18	180.91	4.97	17.04	0.033	1.19	10.9	0.242	243	118	16
17H-6, 127–129	161.28	181.01	6.20	15.43	0.040	1.39	12.7	0.340	268	134	21
17H-6, 137–139	161.38	181.11	6.74	14.61	0.035	1.35	13.7	0.367	293	85	20
17H-6, 147–149	161.48	181.21	4.99	17.25	0.026	1.06	9.9	0.234	235	53	19
154-926B-											
18H-2, 74-76	161.25	181.29	4.16	17.36	0.037	1.02	8.8	0.207	204	86	10
18H-2, 84–86	161.35	181.39	5.97	15.66	0.031	1.41	12.1	0.295	254	127	17
18H-2, 94–96	161.45	181.49	6.45	14.45	0.030	1.44	13.2	0.323	251	86	19
25H-1, 54–56	226.05	252.06	6.83	15.55	0.048	1.10	12.5	0.336	231	58	31
25H-1, 64–66	226.15	252.16	5.16	21.07	0.035	0.75	8.6	0.233	221	82	23
25H-1, 74–76	226.25	252.26	7.80	15.14	0.043	1.20	13.4	0.371	240	193	33
25H-1, 84–86	226.35	252.36	5.79	19.84	0.036	0.80	9.8	0.265	219	216	40
25H-1, 94–96	226.45	252.46	8.19	12.60	0.044	1.41	15.0	0.430	266	106	27
25H-1, 104–106	226.55	252.56	5.19	19.74	0.041	0.80	9.1	0.239	204	69	27
25H-1, 114–116	226.65	252.66	7.15	15.00	0.047	1.16	12.5	0.347	230	70	33
25H-1, 126–128	226.75	252.76	7.89	14.03	0.045	1.21	13.5	0.364	230	61	30
25H-1, 134–136	226.85	252.86	5.61	19.68	0.041	0.79	9.1	0.249	184	108	34
25H-1, 144–146	226.95	252.96	6.16	17.30	0.037	1.00	10.6	0.284	186	67	20
154-926A-											
26H-1, 44–46	232.45	260.81	6.52	24.12	0.035	0.84	10.1	0.263	240	71	22
26H-1, 54–56	232.55	260.91	7.61	13.46	0.052	1.03	12.9	0.337	249	99	37
26H-1, 64–66	232.65	261.01	8.37	18.62	0.049	1.17	13.3	0.343	273	96	20
26H-1, 74–76	232.75	261.11	6.07	24.41	0.041	0.92	10.0	0.268	198	75	33
26H-1, 84–86	232.85	261.21	5.17	26.80	0.035	0.81	8.8	0.224	174	28	26
26H-1, 94–96	232.95	261.31	6.82	22.72	0.031	0.95	11.9	0.303	276	38	73
26H-1, 104–106	233.05	261.41	5.77	26.70	0.024	0.74	9.3	0.240	258	61	37
26H-1, 114–116	233.15	261.51	5.02	26.70	0.029	0.78	8.5	0.211	223	44	93
26H-1, 124–126	233.25	261.61	7.19	22.04	0.047	1.13	12.5	0.320	255	51	35
26H-1, 134–136	233.35	261.71	5.11	26.29	0.033	0.83	9.0	0.230	228	27	27
26H-1, 144–146	233.45	261.81	4.32	30.60	0.036	0.64	6.8	0.177	160	19	20
26H-2, 4–6	233.55	261.91	8.96	12.25	0.053	1.19	17.1	0.522	308	142	37
26H-2, 14–16	233.65	262.01	5.77	19.91	0.038	0.91	10.6	0.278	243	91	25
26H-2, 24–26	233.75	262.11	7.38	15.44	0.049	1.12	13.7	0.359	232	110	48
26H-2, 34–36	233.85	262.21	4.55	21.82	0.036	0.73	8.4	0.229	159	117	23
26H-2, 44–46	233.95	262.31	3.51	22.97	0.033	0.47	6.8	0.161	126	20	21
26H-2, 54–56	234.05	262.41	8.32	17.15	0.052	1.37	16.3	0.409	298	94	23
26H-2, 64–66	234.15	262.51	3.59	22.64	0.035	0.62	6.4	0.174	190	39	24
26H-2, 74–76	234.25	262.61	4.28	23.39	0.042	0.77	8.5	0.207	194	61	34
26H-2, 84–86	234.35	262.71	4.93	22.26	0.043	0.82	8.9	0.245	166	69	34
26H-2, 94–96	234.45	262.81	6.51	20.46	0.040	0.98	11.7	0.303	271	61	20
26H-2, 104–106	234.55	262.91	8.94	16.42	0.050	1.26	16.6	0.433	355	104	76
26H-2, 115–117	234.66	263.02	6.34	17.14	0.054	0.97	11.8	0.310	219	92	17

Table 3 (continued).

Core, section, interval (cm)	Depth (mbsf)	Depth (mcd)	Al (%)	Ca (%)	P (%)	K (%)	Si (%)	Ti (%)	Ba (ppm)	V (ppm)	Cu (ppm)
26H-2, 124–126	234.75	263.11	9.30	15.80	0.056	1.48	17.7	0.462	325	112	39
26H-2, 134–136	234.85	263.21	6.16	17.42	0.054	0.93	11.3	0.287	212	65	22
26H-2, 144–146	234.95	263.31	9.44	15.64	0.058	1.63	18.5	0.482	366	100	23
26H-3, 4–6	235.05	263.41	4.32	17.71	0.030	0.72	7.9	0.194	165	50	23
26H-3, 14–16	235.15	263.51	5.05	17.51	0.030	0.79	9.3	0.237	194	63	23
26H-3, 24–26	235.25	263.61	6.54	15.02	0.040	1.06	12.4	0.309	307	176	30
26H-3, 34–36	235.35	263.71	4.31	17.66	0.045	0.80	8.0	0.191	213	57	26
26H-3, 44–46	235.45	263.81	4.25	17.83	0.039	0.74	7.8	0.198	167	104	44
26H-3, 54–56	235.55	263.91	4.95	20.99	0.035	0.80	9.2	0.251	207	74	24
26H-3, 64–66	235.65	264.01	6.85	14.16	0.041	1.13	13.1	0.336	286	229	28
26H-3, 74–76	235.75	264.11	4.78	24.11	0.043	0.87	9.0	0.218	190	38	32
26H-3, 84–86	235.85	264.21	4.39	26.22	0.033	0.84	8.3	0.209	172	30	22
26H-3, 94–96	235.95	264.31	4.83	24.43	0.031	0.92	9.6	0.238	244	36	24
26H-3, 104–106	236.05	264.41	6.91	13.95	0.033	1.09	12.8	0.330	280	125	44
26H-3, 114–116	236.15	264.51	6.29	14.90	0.032	0.95	11.8	0.297	311	101	38
26H-3, 124–126	236.25	264.61	5.61	23.39	0.032	0.93	9.7	0.245	225	27	28
26H-3, 134–136	236.35	264.71	4.73	17.79	0.026	0.84	8.2	0.207	181	55	30
26H-3, 144–146	236.45	264.81	4.35	25.66	0.030	0.80	8.1	0.217	180	42	26
26H-4, 4–6	236.55	264.91	7.62	17.99	0.053	1.41	14.0	0.355	266	87	112
26H-4, 14–16	236.65	265.01	8.26	14.15	0.049	1.36	15.6	0.408	342	121	39
26H-4, 24–26	236.75	265.11	5.12	22.50	0.031	0.89	9.0	0.217	206	69	26
26H-4, 34–36	236.85	265.21	4.31	20.67	0.033	0.66	8.0	0.214	183	74	21
26H-4, 44–46	236.95	265.31	3.62	19.52	0.038	0.45	6.7	0.172	152	41	30
26H-4, 54–56	237.05	265.41	4.84	19.22	0.033	0.77	8.9	0.232	175	69	30
26H-4, 64–66	237.15	265.51	8.29	10.89	0.049	0.95	16.2	0.413	286	82	36
26H-4, 74–76	237.25	265.61	6.12	15.80	0.037	0.69	11.3	0.293	235	76	24
26H-4, 84–86	237.35	265.71	3.92	20.46	0.038	0.64	7.4	0.196	193	47	16
26H-4, 96–98	237.47	265.83	5.64	16.94	0.045	0.64	10.6	0.283	221	57	90
26H-4, 108–110	237.59	265.95	6.32	16.80	0.028	0.88	11.6	0.320	237	63	82
26H-4, 115–117	237.66	266.02	6.54	14.58	0.041	0.72	12.2	0.312	219	83	33
26H-4, 124–126	237.75	266.11	10.27	10.12	0.065	1.51	19.2	0.477	351	147	55
26H-4, 134–136	237.85	266.21	6.38	16.23	0.040	1.05	12.3	0.348	255	104	24
26H-4, 144–146	237.95	266.31	2.99	28.01	0.030	0.67	5.7	0.133	121	48	24
154-926B-											
50X-1, 14–16	461.55	491.36	4.48	14.73	0.049	0.69	10.2	0.177	818	57	26
50X-1, 24–26	461.65	491.46	4.57	14.50	0.043	0.70	10.5	0.179	672	52	38
50X-1, 34–36	461.75	491.56	3.89	15.37	0.046	0.61	9.1	0.153	611	48	24
50X-1, 44–46	461.85	491.66	3.93	15.23	0.039	0.64	9.2	0.157	768	62	30
50X-1, 52–54	461.93	491.74	3.26	15.87	0.043	0.61	7.8	0.136	708	52	19
50X-1, 64–66	462.05	491.86	3.40	16.28	0.045	0.49	7.4	0.138	699	38	20
50X-1, 74–76	462.15	491.96	2.98	16.17	0.032	0.50	7.5	0.118	788	32	22
50X-1, 85–87	462.26	492.07	3.30	16.71	0.036	0.43	8.0	0.132	697	31	24
50X-1, 94–96	462.35	492.16	3.07	16.09	0.039	0.53	7.2	0.126	700	70	38
50X-1, 105–107	462.45	492.26	3.82	15.62	0.047	0.52	8.7	0.163	765	72	23
50X-1, 114–116	462.55	492.36	4.54	17.54	0.069	0.59	10.7	0.225	810	28	30
50X-1, 124–126	462.65	492.46	5.23	14.65	0.060	0.62	11.6	0.224	772	70	38
50X-1, 134–136	462.75	492.56	5.61	14.15	0.047	0.73	12.5	0.246	796	70	29
50X-1, 144–146	462.85	492.66	5.35	14.45	0.050	0.73	12.1	0.223	779	80	36
50X-2, 4–6	462.95	492.76	3.68	13.35	0.042	0.52	8.8	0.147	703	79	26
50X-2, 14–16	463.05	492.86	3.50	16.73	0.037	0.54	8.6	0.155	596	50	24
50X-2, 24–26	463.15	492.96	3.35	18.58	0.026	0.55	8.2	0.147	612	49	57
50X-2, 34–36	463.25	493.06	4.35	12.88	0.027	0.51	9.9	0.174	781	56	28
50X-2, 44–46	463.35	493.16	4.39	17.13	0.027	0.63	10.6	0.196	818	80	64
50X-2, 54–56	463.45	493.26	4.89	17.65	0.028	0.66	11.4	0.226	864	45	53
50X-2, 64–66	463.55	493.36	5.06	12.22	0.036	0.59	11.0	0.216	756	77	74
50X-2, 74–76	463.65	493.46	4.82	12.74	0.047	0.55	10.3	0.210	717	67	33
50X-2, 84–86	463.75	493.56	6.71	13.32	0.043	0.77	14.6	0.364	861	85	43
50X-2, 94–96	463.85	493.66	5.41	14.70	0.037	0.69	12.5	0.283	813	77	25
50X-2, 104–106	463.95	493.76	3.10	13.52	0.033	0.56	7.5	0.129	606	46	61
50X-2, 114–116	464.05	493.86	3.03	19.51	0.040	0.54	7.4	0.133	514	47	34
50X-2, 124–126	464.15	493.96	3.91	16.45	0.047	0.57	9.3	0.173	751	52	18
50X-2, 134–136	464.25	494.06	3.49	17.17	0.042	0.68	9.8	0.172	809	56	17
50X-2, 146–148	464.37	494.18	3.78	16.79	0.022	0.51	9.5	0.178	685	52	47
50X-3, 4–6	464.45	494.26	2.73	22.61	0.020	0.39	6.7	0.136	598	56	41
50X-3, 14–16	464.55	494.36	3.93	18.36	0.023	0.55	9.4	0.157	633	40	30
50X-3, 24–26	464.65	494.46	4.14	19.50	0.027	0.59	9.6	0.210	651	81	46
50X-3, 30–32	464.75	494.56	4.96	17.41	0.033	0.66	11.7	0.246	720	84	57
50X-3, 44–46	464.85	494.66	3.80	18.58	0.092	0.62	9.7	0.169	649	53	58
50X-3, 54–56	464.95	494.76	3.43	19.11	0.066	0.56	9.0	0.136	641	43	43
50X-3, 64–66	465.05	494.86	2.98	22.05	0.055	0.55	7.2	0.128	572	53	34
50X-3, 73–75	465.14	494.95	2.99	18.86	0.043	0.53	7.7	0.122	610	51	25
50X-3, 84–86	465.25	495.06	3.54	18.52	0.035	0.51	9.5	0.164	608	109	31
50X-3, 93–95	465.35	495.16	3.93	18.43	0.043	0.66	9.7	0.151	765	45	31
50X-3, 104–106	465.45	495.26	3.65	20.61	0.041	0.69	8.9	0.173	681	71	43
50X-3, 114–116	465.55	495.36	5.00	17.41	0.056	0.91	12.2	0.224	687	90	42
50X-3, 124–126	465.65	495.46	5.62	16.51	0.050	0.78	13.6	0.230	859	79	43
50X-3, 134–136	465.75	495.56	6.85	15.71	0.053	0.84	16.2	0.300	755	86	54
50X-3, 144–146	465.85	495.66	5.79	16.90	0.070	0.89	13.3	0.241	704	66	35
50X-4, 4–6	465.95	495.76	3.73	19.45	0.045	0.86	9.2	0.159	747	87	85
50X-4, 14–16	466.05	495.86	5.08	22.98	0.059	0.78	12.9	0.227	787	109	88
50X-4, 24–26	466.15	495.96	4.22	18.91	0.053	0.92	10.1	0.169	683	59	80
50X-4, 32–34	466.23	496.04	4.15	23.60	0.048	0.80	10.9	0.195	889	89	47
50X-4, 44–46	466.35	496.16	5.00	22.82	0.058	0.73	12.0	0.199	878	65	39
50X-4, 54–56	466.45	496.26	4.40	18.56	0.056	0.68	10.2	0.206	801	53	66
50X-4, 64–66	466.55	496.36	7.23	20.34	0.051	0.89	16.3	0.311	1277	123	58
50X-4, 74–76	466.65	496.46	7.34	16.68	0.052	1.01	16.5	0.339	1037	128	33
50X-4, 84–86	466.75	496.56	5.58	18.87	0.084	0.74	12.8	0.219	1002	84	23
50X-4, 96–98	466.85	496.66	4.90	22.44	0.069	0.72	12.2	0.214	946	55	48
50X-4, 104–106	466.95	496.76	5.03	21.07	0.051	0.66	10.8	0.185	860	84	23
50X-4, 114–116	467.05	496.86	4.04	19.01	0.047	0.63	9.9	0.173	857	37	29

Table 3 (continued).

Core, section, interval (cm)	Depth (mbsf)	Depth (mcd)	Al (%)	Ca (%)	P (%)	K (%)	Si (%)	Ti (%)	Ba (ppm)	V (ppm)	Cu (ppm)
50X-4, 124–126	467.15	496.96	3.40	19.50	0.042	0.62	9.3	0.148	872	20	33
50X-4, 134–136	467.25	497.06	4.40	20.36	0.055	0.66	10.4	0.187	1087	52	25
50X-4, 144–146	467.35	497.16	4.99	21.25	0.042	0.70	10.5	0.178	1052	95	32
50X-5, 4–6	467.45	497.26	3.44	16.31	0.038	0.54	8.3	0.159	840	58	29
50X-5, 14–16	467.55	497.36	3.81	14.34	0.048	0.52	8.7	0.160	777	52	31
50X-5, 24–26	467.65	497.46	4.52	15.05	0.040	0.56	10.2	0.218	939	66	46
50X-5, 32–34	467.73	497.54	4.86	13.36	0.037	0.66	10.7	0.214	871	71	36
50X-5, 44–46	467.85	497.66	4.29	15.21	0.061	0.47	9.9	0.198	697	58	31
50X-5, 52–54	467.93	497.74	4.43	14.96	0.039	0.60	10.1	0.204	718	55	107
50X-5, 64–66	468.05	497.86	3.32	21.04	0.045	0.50	7.9	0.151	731	53	38
50X-5, 74–76	468.15	497.96	2.83	16.66	0.037	0.42	6.8	0.126	807	35	34
50X-5, 84–86	468.25	498.06	2.66	15.09	0.029	0.45	6.4	0.110	797	51	42
50X-5, 96–98	468.37	498.18	2.99	21.65	0.024	0.42	7.2	0.139	695	60	48
50X-5, 104–106	468.45	498.26	2.78	16.76	0.032	0.38	6.3	0.125	598	33	46
50X-5, 114–116	468.55	498.36	2.94	16.40	0.038	0.39	6.9	0.133	617	35	22
50X-5, 124–126	468.65	498.46	3.56	16.29	0.037	0.47	8.5	0.162	865	63	32
50X-5, 134–136	468.75	498.56	3.85	15.74	0.040	0.48	9.1	0.182	835	58	38
50X-5, 144–146	468.85	498.66	3.64	16.26	0.043	0.50	8.3	0.169	790	50	29
50X-6, 4–6	468.95	498.76	5.05	17.46	0.037	0.67	13.4	0.214	1057	44	41
50X-6, 14–16	469.05	498.86	5.56	17.41	0.040	0.67	12.5	0.211	979	47	31
50X-6, 22–24	469.13	498.94	6.28	16.57	0.037	0.79	15.0	0.252	1108	73	35
50X-6, 34–36	469.25	499.06	5.44	16.64	0.045	0.69	12.0	0.223	930	102	14
50X-6, 46–48	469.37	499.18	4.02	14.89	0.038	0.54	9.0	0.171	775	52	19
50X-6, 54–56	469.45	499.26	4.83	13.73	0.038	0.61	10.9	0.209	835	64	81
50X-6, 64–66	469.55	499.36	5.61	17.56	0.039	0.67	13.1	0.221	1046	57	36
50X–6, 74–76	469.65	499.46	4.18	17.77	0.043	0.58	9.8	0.177	894	74	43
50X-6, 84–86	469.75	499.56	3.28	13.36	0.030	0.41	7.6	0.143	625	42	20
50X-6, 94–96	469.85	499.66	5.50	16.47	0.045	0.62	12.1	0.217	858	67	49
50X-6, 104–106	469.95	499.76	5.97	16.24	0.048	0.76	12.5	0.239	931	71	26
50X-6, 114–116	470.05	499.86	4.77	14.04	0.038	0.58	10.6	0.202	818	66	27
50X-6, 124–126	470.15	499.96	6.04	16.11	0.047	0.74	12.9	0.243	1020	74	63
50X-6, 134–136	470.25	500.06	4.58	13.89	0.034	0.57	10.0	0.192	852	64	38
50X-CC, 4–6	470.35	500.16	3.58	16.73	0.056	0.55	8.2	0.168	735	76	29
50X-CC, 14–16	470.45	500.26	3.57	17.23	0.045	0.52	8.0	0.156	633	33	28
50X-CC, 24–26	470.55	500.36	3.75	16.77	0.047	0.50	8.0	0.164	728	33	41
50X-CC, 34–36	470.65	500.46	4.15	15.76	0.044	0.59	9.2	0.183	923	54	40
50X-CC, 44–46	470.75	500.56	4.44	15.24	0.049	0.55	10.5	0.200	853	65	29
51X-1, 14–16	471.15	500.96	4.70	16.76	0.034	0.48	10.2	0.194	732	63	37
51X-1, 24–26	471.25	501.06	4.90	16.04	0.028	0.52	11.5	0.219	991	74	81
51X-1, 33–35	471.34	501.15	5.75	21.66	0.045	0.83	13.7	0.288	1271	79	77
51X-1, 44–46	471.45	501.26	3.98	24.29	0.050	0.68	9.5	0.179	1058	61	14
51X-1, 54–56	471.55	501.36	2.96	18.27	0.043	0.49	6.8	0.127	650	48	24
51X-1, 64–66	471.65	501.46	3.10	17.88	0.050	0.46	7.1	0.138	569	53	36
51X-1, 74–76	471.75	501.56	3.64	16.83	0.037	0.41	8.9	0.163	779	60	31
51X-1, 84–86	471.85	501.66	4.40	16.23	0.034	0.56	9.7	0.196	896	74	59
51X-1, 93–95	471.94	501.75	5.26	18.38	0.045	0.66	12.4	0.246	920	81	35
51X-1, 104–106	472.05	501.86	5.64	17.55	0.052	0.66	12.8	0.262	929	82	33
51X-1, 114–116	472.15	501.96	5.56	18.13	0.044	0.66	12.6	0.258	909	82	21
51X-1, 124–126	472.25	502.06	5.69	17.67	0.032	0.71	12.5	0.258	914	72	39
51X-1, 134–136	472.35	502.16	6.01	17.43	0.032	0.71	13.1	0.272	973	69	31
51X-1, 144–146	472.45	502.26	4.52	15.96	0.039	0.47	9.8	0.195	720	64	76
51X-2, 6–8	472.57	502.38	4.59	18.92	0.026	0.60	10.8	0.208	762	66	50
51X-2, 14–16	472.65	502.46	3.51	19.24	0.037	0.59	8.0	0.149	735	54	35
51X-2, 24–26	472.75	502.56	3.33	20.56	0.035	0.78	7.7	0.140	682	49	23
51X-2, 33–35	472.84	502.65	3.98	19.41	0.036	0.95	8.6	0.167	806	52	35
51X-2, 44–46	472.95	502.76	3.70	20.04	0.036	0.86	8.1	0.156	630	41	25
51X-2, 54–56	473.05	502.86	4.27	20.35	0.031	0.60	8.8	0.192	672	65	35
51X-2, 64–66	473.15	502.96	5.45	17.21	0.037	0.71	12.3	0.263	995	85	47
51X-2, 74–76	473.25	503.06	5.92	17.18	0.043	0.77	10.9	0.233	921	78	39
51X-2, 84–86	473.35	503.16	4.36	19.48	0.044	0.78	10.5	0.204	944	64	35
51X-2, 94–96	473.45	503.26	4.39	19.47	0.045	0.63	8.9	0.178	745	82	38
51X-2, 104–106	473.55	503.36	3.05	21.90	0.041	0.68	7.4	0.133	568	60	38
51X-2, 114–116	473.65	503.46	3.28	21.30	0.032	0.56	8.6	0.156	688	53	33
51X-2, 124–126	473.75	503.56	3.81	20.26	0.036	0.73	9.1	0.173	895	60	46
51X-2, 134–136	473.85	503.66	2.82	22.02	0.034	0.60	6.9	0.132	766	59	34
51X-2, 144–146	473.95	503.76	2.95	21.61	0.028	0.44	7.4	0.141	740	43	26
51X-3, 3–5	474.04	503.85	3.18	22.78	0.035	0.55	7.9	0.145	622	49	26
51X-3, 14–16	474.15	503.96	3.33	23.28	0.031	0.70	8.1	0.151	563	45	34
51X-3, 24–26	474.25	504.06	5.09	19.36	0.027	0.63	11.9	0.245	829	72	41
51X-3, 33–35	474.34	504.15	6.27	15.32	0.030	0.80	13.7	0.370	932	84	47
51X-3, 44–46	474.45	504.26	4.67	20.25	0.063	0.63	11.5	0.218	958	69	42
51X-3, 54–56	474.55	504.36	4.44	20.52	0.037	0.50	10.8	0.221	971	70	46
51X-3, 64–66	474.65	504.46	3.61	21.99	0.035	0.67	8.7	0.164	685	57	36
51X-3, 74–76	474.75	504.56	3.13	21.72	0.036	0.64	7.4	0.150	627	58	27
51X-3, 82–84	474.85	504.66	3.92	20.50	0.035	0.55	9.3	0.181	736	68	41
51X-3, 94–96	474.95	504.76	3.98	21.89	0.035	0.37	9.6	0.200	756	66	28
51X-3, 104–106	475.05	504.86	3.11	22.91	0.030	0.53	8.0	0.150	804	46	33
51X-3, 114–116	475.15	504.96	3.31	21.97	0.035	0.40	8.1	0.158	860	46	42
51X-3, 124–126	475.25	505.06	3.95	21.50	0.029	0.45	9.7	0.188	719	57	33
51X-3, 134–136	475.35	505.16	3.95	20.32	0.026	0.68	9.6	0.189	644	56	32
51X-4, 4–6	475.55	505.36	4.75	20.97	0.043	0.63	11.4	0.223	843	92	34
51X-4, 14–16	475.65	505.46	5.00	18.52	0.038	0.69	11.5	0.244	991	74	40
51X-4, 24–26	475.75	505.56	4.24	22.12	0.048	0.65	10.2	0.198	941	56	43
51X-4, 33–35	475.84	505.65	3.65	22.86	0.040	0.48	9.1	0.171	792	76	24
51X-4, 47–49	475.98	505.79	3.32	23.75	0.040	0.55	8.4	0.154	690	42	34
51X-4, 54–56	476.05	505.86	3.30	23.57	0.029	0.50	8.0	0.150	566	47	30
51X-4, 64–66	476.15	505.96	2.90	22.51	0.028	0.46	7.4	0.131	582	41	24
51X-4, 74–76	476.25	506.06	4.18	22.10	0.026	0.61	10.1	0.201	891	79	24
51X-4, 84–86	476.35	506.16	4.43	21.45	0.030	0.66	10.7	0.215	1038	83	55
51X-4, 93–95	476.44	506.25	3.97	22.39	0.034	0.61	9.8	0.189	918	108	30
51X-4, 104–106	476.55	506.36	3.94	22.56	0.026	0.65	9.6	0.177	851	65	34

Table 3 (continued).

Core, section, interval (cm)	Depth (mbsf)	Depth (mcd)	Al (%)	Ca (%)	P (%)	K (%)	Si (%)	Ti (%)	Ba (ppm)	V (ppm)	Cu (ppm)
51X-4, 114–116	476.65	506.46	3.10	21.82	0.032	0.52	7.5	0.139	712	75	34
51X-4, 124–126	476.75	506.56	4.24	20.01	0.032	0.61	9.8	0.206	958	45	49
51X-4, 136–138	476.87	506.68	3.82	19.98	0.033	0.64	9.5	0.180	832	54	63
51X-4, 144–146	476.95	506.76	2.83	22.32	0.037	0.60	7.4	0.130	697	70	35
51X-5, 4–6	477.05	506.86	3.40	26.28	0.039	0.70	9.1	0.154	776	99	55
51X-5, 14–16	477.15	506.96	3.72	18.95	0.023	0.56	9.2	0.172	700	46	26
51X-5, 24–26	477.25	507.06	5.24	15.03	0.033	0.82	14.3	0.254	866	78	33
51X-5, 33–35	477.34	507.15	6.76	20.37	0.037	1.02	17.0	0.329	1166	116	45
51X-5, 44–46	477.45	507.26	4.67	17.18	0.050	0.76	11.2	0.220	878	84	39
51X-5, 52–54	477.55	507.36	3.93	18.90	0.038	0.58	9.6	0.177	876	71	36
51X-5, 64–66	477.65	507.46	4.94	23.70	0.059	0.77	12.3	0.230	843	70	29
51X-5, 74–76	477.75	507.56	5.18	22.84	0.048	0.82	12.9	0.244	891	71	31
51X-5, 84–86	477.85	507.66	3.79	18.63	0.031	0.56	9.2	0.177	693	65	30
51X-5, 93–95	477.94	507.75	3.28	20.00	0.035	0.46	7.9	0.151	685	51	48
51X-5, 104–106	478.05	507.86	4.09	24.58	0.045	0.60	10.6	0.193	858	66	24
51X-5, 114–116	478.15	507.96	3.61	19.20	0.030	0.50	8.9	0.164	715	61	30
51X-5, 124–126	478.25	508.06	4.07	18.84	0.033	0.58	9.8	0.187	777	63	25
51X-5, 134–136	478.35	508.16	4.86	17.50	0.039	0.74	11.5	0.230	890	81	39
51X-5, 144–145	478.45	508.26	5.14	16.82	0.034	0.80	12.3	0.254	898	76	35
51X-6, 4–6	478.55	508.36	4.40	18.75	0.046	0.66	10.5	0.189	863	63	29
51X-6, 14–16	478.65	508.46	3.85	16.26	0.036	0.61	8.6	0.176	648	52	47
51X-6, 24–26	478.75	508.56	3.65	16.57	0.043	0.60	8.7	0.172	565	60	37
51X-6, 33–35	478.84	508.65	3.41	16.67	0.040	0.67	8.3	0.153	550	59	33
51X-6, 44–46	478.95	508.76	5.05	22.68	0.053	0.89	12.5	0.230	959	64	63
51X-6, 54–56	479.05	508.86	5.38	21.87	0.043	0.93	13.3	0.257	914	76	24
51X-6, 64–66	479.15	508.96	4.46	15.50	0.033	0.72	10.4	0.202	737	69	43
51X-6, 74–76	479.25	509.06	5.22	22.45	0.044	0.74	12.4	0.240	918	76	65
51X-6, 84–86	479.35	509.16	4.22	15.31	0.032	0.60	10.1	0.204	700	66	55
51X-6, 94–96	479.45	509.26	4.50	15.37	0.031	0.69	10.5	0.215	689	67	43
51X-6, 104–106	479.55	509.36	3.88	19.27	0.036	0.63	9.2	0.168	749	58	10
51X-6, 114–116	479.65	509.46	2.87	16.83	0.034	0.52	7.3	0.132	573	49	43
51X-6, 124–126	479.75	509.56	3.01	20.37	0.037	0.57	7.3	0.134	657	51	41
51X-6, 134–136	479.85	509.66	2.98	20.22	0.041	0.52	7.3	0.131	712	40	43
51X-6, 144–146	479.95	509.76	3.38	19.68	0.036	0.53	8.3	0.148	686	48	12
51X-7, 4–6	480.05	509.86	4.42	17.02	0.043	0.65	10.5	0.199	690	60	34
51X-7, 14–16	480.15	509.96	4.36	15.92	0.045	0.63	10.4	0.204	680	65	31
51X-7, 24–26	480.25	510.06	5.44	15.47	0.040	0.71	12.7	0.237	822	64	45
51X-7, 33–35	480.34	510.15	5.06	16.15	0.051	0.69	11.7	0.227	880	73	39
51X-CC, 4–6	480.45	510.26	3.55	17.21	0.038	0.56	8.0	0.168	786	113	33
51X-CC, 14–16	480.55	510.36	3.38	17.60	0.036	0.52	7.9	0.158	632	61	29
51X-CC, 24–26	480.65	510.46	3.21	17.73	0.033	0.53	7.8	0.152	778	58	18
51X-CC, 34–36	480.75	510.56	3.21	17.59	0.035	0.59	8.0	0.156	695	54	22
64X-1, 4–6	596.55	626.36	3.36	22.16	0.038	0.53	7.4	0.148	739	75	46
64X-1, 14–15	596.65	626.46	2.83	22.80	0.043	0.49	6.1	0.118	744	66	25
64X-1, 24–26	596.75	626.56	2.51	22.89	0.035	0.38	5.8	0.115	805	69	59
64X-1, 35–36	596.86	626.67	1.88	24.16	0.031	0.31	4.2	0.086	760	37	32
64X-1, 44–46	596.95	626.76	1.86	23.55	0.026	0.27	4.4	0.084	760	60	50
64X-1, 54–55	597.05	626.86	2.09	18.91	0.034	0.32	4.8	0.097	634	33	17
64X-1, 64–66	597.15	626.96	1.97	19.11	0.034	0.33	4.7	0.091	530	51	9
64X-1, 74–75	597.25	627.06	2.38	22.43	0.024	0.38	5.8	0.109	582	60	60
64X-1, 84–86	597.35	627.16	3.36	22.23	0.035	0.56	7.6	0.168	692	49	31
64X-1, 94–95	597.45	627.26	2.96	17.84	0.040	0.46	7.0	0.140	648	43	14
64X-1, 104–106	597.55	627.36	3.00	17.46	0.032	0.48	7.2	0.144	598	39	18
64X-1, 114–115	597.65	627.46	2.56	23.56	0.029	0.43	5.5	0.109	659	47	48
64X-1, 124–126	597.75	627.56	2.30	23.90	0.037	0.42	5.0	0.097	678	37	47
64X-1, 134–135	597.85	627.66	2.14	18.52	0.033	0.36	5.1	0.100	611	23	6
64X-1, 143–145	597.94	627.75	2.20	23.26	0.030	0.42	5.1	0.097	715	80	48
64X-2, 4–5	598.05	627.86	2.10	18.36	0.039	0.37	5.3	0.096	656	98	25
64X-2, 14–16	598.15	627.96	1.66	18.99	0.046	0.36	4.6	0.079	492	71	18
64X-2, 24–25	598.25	628.06	1.93	18.85	0.038	0.35	5.0	0.092	775	49	29
64X-2, 34–36	598.35	628.16	2.60	18.37	0.033	0.43	6.2	0.119	692	41	31
64X-2, 44–45	598.45	628.26	3.17	17.75	0.038	0.54	7.2	0.145	751	34	25
64X-2, 54–56	598.55	628.36	3.37	17.60	0.035	0.57	7.8	0.154	721	34	26
64X-2, 64–65	598.65	628.46	4.09	16.33	0.040	0.66	9.8	0.192	806	107	39
64X-2, 74–76	598.75	628.56	4.92	15.90	0.038	0.76	11.4	0.235	825	73	38
64X-2, 84–86	598.85	628.66	4.12	16.22	0.028	0.69	9.4	0.191	876	100	23
64X-2, 94–96	598.95	628.76	3.45	17.62	0.036	0.59	8.2	0.161	822	63	36
64X-2, 104–105	599.05	628.86	2.82	19.94	0.033	0.49	6.8	0.124	771	40	16
64X-2, 114–116	599.15	628.96	2.28	19.03	0.028	0.33	5.5	0.100	741	81	27
64X-2, 124–125	599.25	629.06	2.25	19.22	0.034	0.42	5.5	0.101	687	38	15
64X-2, 134–136	599.35	629.16	2.19	19.22	0.031	0.39	5.3	0.095	765	70	20
64X-2, 146–147	599.45	629.26	2.10	19.41	0.030	0.39	5.0	0.094	754	57	16
64X-3, 4–6	599.55	629.36	3.00	21.72	0.043	0.43	7.1	0.120	964	41	29
64X-3, 14–16	599.65	629.46	3.47	20.58	0.048	0.45	8.0	0.137	918	48	47
64X-3, 24–26	599.75	629.56	3.32	20.62	0.044	0.52	7.6	0.133	860	40	24
64X-3, 33–34	599.84	629.65	3.43	20.77	0.045	0.48	7.6	0.136	756	50	21
64X-3, 43–45	599.94	629.75	3.98	21.29	0.038	0.52	8.4	0.163	946	47	24
64X-3, 54–56	600.05	629.86	8.76	15.06	0.029	0.64	16.1	0.637	873	128	35
64X–3, 67–69	600.18	629.99	4.04	20.70	0.059	0.65	9.2	0.190	1192	51	31
64X-3, 74–76	600.25	630.06	2.39	22.56	0.048	0.44	6.0	0.089	1004	40	19
64X-3, 84–86	600.35	630.16	1.69	21.74	0.042	0.37	4.3	0.070	665	23	21
64X-3, 94–96	600.45	630.26	1.68	22.02	0.038	0.35	4.2	0.066	544	35	15
64X-3, 105–107	600.56	630.37	1.75	18.62	0.026	0.32	4.2	0.074	569	30	15
64X-3, 114–116	600.65	630.46	3.11	19.76	0.038	0.52	7.5	0.128	878	59	36
64X-3, 124–126	600.75	630.56	4.19	19.30	0.048	0.68	9.9	0.177	960	56	34
64X-3, 134–136	600.85	630.66	4.06	19.00	0.046	0.65	9.1	0.170	965	62	36
64X-3, 144–146	600.95	630.76	4.57	18.55	0.050	0.68	10.4	0.187	919	67	41
64X-4, 4–5	601.05	630.86	3.45	18.53	0.036	0.57	8.0	0.156	784	116	26
64X-4, 14–16	601.15	630.96	2.89	13.97	0.031	0.50	6.9	0.132	682	37	61
64X-4, 24–26	601.25	631.06	3.07	18.85	0.041	0.51	7.7	0.145	933	66	23
64X-4, 32–34	601.33	631.14	2.15	20.37	0.034	0.40	5.5	0.103	780	95	24

Table 3 (continued).

Core, section, interval (cm)	Depth (mbsf)	Depth (mcd)	Al (%)	Ca (%)	P (%)	K (%)	Si (%)	Ti (%)	Ba (ppm)	V (ppm)	Cu (ppm)
64X-4, 44–46	601.45	631.26	1.85	16.23	0.036	0.43	4.8	0.091	682	45	64
64X-4, 54–56	601.55	631.36	2.43	19.25	0.038	0.36	6.0	0.111	751	36	15
64X-4, 64–65	601.65	631.46	2.83	18.70	0.036	0.49	6.8	0.131	803	39	19
64X-4, 72–74	601.73	631.54	3.48	18.95	0.029	0.59	8.1	0.159	868	67	43
64X-4, 84–85	601.85	631.66	4.37	16.50	0.046	0.69	10.2	0.197	933	61	22
64X-4, 94–96	601.95	631.76	4.70	13.03	0.033	0.73	11.2	0.228	925	66	69
64X-4, 104–105	602.05	631.86	3.98	18.17	0.029	0.62	10.0	0.173	921	105	29
64X-4, 114–116	602.15	631.96	1.93	13.56	0.032	0.42	4.7	0.083	586	30	62
64X-4, 124–126	602.25	632.06	1.69	19.58	0.041	0.33	4.4	0.073	677	31	10
64X-4, 134–136	602.35	632.16	1.57	19.65	0.043	0.30	4.3	0.071	717	30	15
64X-4, 143–144	602.44	632.25	1.44	21.82	0.030	0.31	3.9	0.067	822	44	14
64X-5, 4–6	602.55	632.36	1.60	19.16	0.032	0.27	4.2	0.076	948	54	33
64X-5, 14–15	602.65	632.46	1.87	19.11	0.026	0.33	4.7	0.089	927	99	33
64X-5, 24–26	602.75	632.56	2.26	18.35	0.028	0.34	5.4	0.108	829	61	35
64X–5, 34–35	602.85	632.66	2.38	18.35	0.031	0.31	5.6	0.112	724	42	40
64X-5, 44–46	602.95	632.76	4.58	15.46	0.038	0.57	10.0	0.257	915	63	33
64X-5, 54–55	603.05	632.86	8.76	15.06	0.029	0.64	16.1	0.658	873	128	35
64X-5, 64–66	603.15	632.96	5.08	13.45	0.022	0.70	10.9	0.302	939	72	40
64X-5, 74–76	603.25	633.06	1.80	18.03	0.036	0.33	4.6	0.074	793	30	17
64X-5, 84–86	603.35	633.16	1.23	19.19	0.035	0.09	3.9	0.073	729	45	17
64X-5, 94–96	603.45	633.26	1.52	18.87	0.029	0.14	4.8	0.093	878	49	51
64X-5, 104–106	603.55	633.36	2.24	17.68	0.030	0.36	5.6	0.099	800	43	28
64X-5, 114–115	603.65	633.46	2.05	17.83	0.029	0.18	6.5	0.125	888	57	40
64X-5, 124–126	603.75	633.56	2.99	16.89	0.031	0.48	7.1	0.133	793	60	36
64X-5, 134–136	603.85	633.66	2.75	16.82	0.033	0.43	8.1	0.166	825	49	26
64X-5, 143–145	603.94	633.75	1.72	10.22	0.019	0.10	5.1	0.105	471	49	23
64X-6, 4–5	604.05	633.86	4.99	15.74	0.029	0.70	12.2	0.252	938	123	43
64X-6, 15–17	604.15	633.96	3.20	18.51	0.043	0.45	7.4	0.139	911	46	28
64X-6, 24–25	604.25	634.06	2.21	19.01	0.034	0.34	5.2	0.098	860	42	24
64X-6, 36–38	604.37	634.18	2.22	19.65	0.040	0.31	5.2	0.097	821	43	20
64X-6, 44–45	604.45	634.26	1.67	19.51	0.033	0.24	4.2	0.070	667	30	20
64X-6, 54–56	604.55	634.36	1.69	20.26	0.027	0.27	4.0	0.070	668	39	24
64X-6, 64–66	604.65	634.46	2.22	23.53	0.035	0.45	5.6	0.104	802	26	34
64X-6, 74–76	604.75	634.56	3.25	24.41	0.037	0.54	7.9	0.152	990	83	26
64X-6, 84–85	604.85	634.66	3.33	17.98	0.027	0.52	7.8	0.145	870	70	40
64X-6, 94–96	604.85	634.76	3.55	21.77	0.035	0.63	8.5	0.168	913	45	35
64X-6, 104–105	604.95	634.86	3.35	18.08	0.035	0.46	7.7	0.143	825	48	29
64X-6, 114–116	605.05	634.96	2.84	23.20	0.035	0.53	6.8	0.138	784	92	30
64X-6, 124–126	605.15	635.06	2.41	24.74	0.035	0.45	6.0	0.111	797	44	23
64X-6, 135–137	605.26	635.17	1.63	20.10	0.033	0.27	4.0	0.071	764	39	19
64X-6, 145–146	605.36	635.27	2.17	19.38	0.033	0.32	4.9	0.091	716	40	27
64X-7, 4–6	605.45	635.36	2.11	25.35	0.031	0.35	5.0	0.100	659	92	16
64X-7, 14–15	605.55	635.46	3.46	23.11	0.032	0.56	7.9	0.160	730	112	26
64X-7, 26–28	605.67	635.58	5.07	17.92	0.022	0.71	10.7	0.246	863	75	36
64X-7, 34–35	605.75	635.66	5.29	17.37	0.028	0.78	12.0	0.283	966	84	31
64X-CC, 1–3	605.82	635.73	3.42	20.90	0.041	0.50	7.6	0.156	884	59	29
64X-CC, 14–15	605.95	635.86	3.95	20.49	0.049	0.52	8.3	0.195	918	47	33
64X-CC, 24–26	606.05	635.96	2.54	22.83	0.024	0.41	5.6	0.109	757	59	23
154-929A-											
47X-1, 0–2	436.11	451.53	1.81	24.00	0.042	0.45	6.1	0.079	921	43	34
47X-1, 10–12	436.21	451.63	2.35	21.75	0.047	0.79	6.9	0.099	919	35	33
47X-1, 20–22	436.31	451.73	2.55	21.82	0.033	0.72	8.0	0.107	932	41	23
47X-1, 30–32	436.41	451.83	3.09	21.14	0.033	0.70	8.5	0.134	1004	48	37
47X-1, 40–42	436.51	451.93	3.43	20.69	0.022	0.81	9.1	0.151	978	67	68
47X-1, 50–52	436.61	452.03	4.17	20.97	0.010	0.76	10.7	0.180	983	63	37
47X-1, 60–62	436.71	452.13	3.68	19.94	0.045	0.67	9.9	0.154	1256	55	50
47X-1, 70–72	436.81	452.23	2.53	22.36	0.051	0.62	7.3	0.113	1064	39	31
47X-1, 80–82	436.91	452.33	2.38	24.54	0.012	0.60	6.9	0.105	936	43	40
47X-1, 90–92	437.01	452.43	2.34	22.63	0.050	0.51	7.2	0.102	991	44	27
47X-1, 100–102	437.11	452.53	2.88	21.93	0.040	0.87	7.9	0.118	839	40	34
47X-1, 110–112	437.21	452.63	3.30	22.80	0.013	0.61	8.7	0.141	887	55	58
47X-1, 120–122	437.31	452.73	3.58	22.35	0.015	0.60	9.6	0.153	977	53	45
47X-1, 130–132	437.41	452.83	4.13	19.50	0.041	0.73	10.5	0.165	1057	63	30
47X-1, 140–142	437.51	452.93	3.87	21.67	0.014	0.77	9.7	0.160	896	54	50
47X-2, 0–2	437.61	453.03	3.44	22.83	0.039	0.41	9.1	0.153	947	55	32
47X-2, 10–12	437.71	453.13	2.85	22.42	0.039	0.31	7.5	0.131	856	45	34
47X–2, 20–22	437.81	453.23	2.62	22.23	0.044	0.29	7.2	0.122	935	46	30
47X-2, 30–32	437.91	453.33	3.49	22.53	0.048	0.33	9.2	0.153	1265	48	42
47X-2, 40–42	438.01	453.43	3.29	22.61	0.044	0.47	9.2	0.141	1077	50	53
47X-2, 50–52	438.11	453.53	3.36	21.27	0.033	0.48	9.1	0.145	975	41	40
47X-2, 60–62	438.21	453.63	5.38	14.16	0.028	0.86	14.3	0.253	1394	94	72
47X-2, 70–72	438.31	453.73	5.23	15.43	0.020	0.77	12.9	0.234	1187	122	75
47X-2, 80–82	438.41	453.83	3.54	21.57	0.031	0.40	9.0	0.160	936	53	50
47X-2, 90–92	438.51	453.93	3.05	23.49	0.051	0.32	8.4	0.143	1027	41	32
47X-2, 100–102	438.61	454.03	2.34	22.83	0.047	0.27	7.2	0.108	935	33	27
47X-2, 110–112	438.71	454.13	1.89	24.90	0.046	0.21	6.7	0.092	845	49	26
47X-2, 120–122	438.81	454.23	1.56	20.85	0.032	0.25	7.2	0.073	716	60	39
47X-2, 130–132	438.91	454.33	1.65	21.07	0.022	0.20	6.1	0.071	650	75	29
47X-2, 140–142	439.01	454.43	2.68	19.44	0.033	0.38	8.0	0.116	895	62	56
47X-3, 10–12	439.21	454.63	5.66	14.88	0.040	0.86	14.2	0.281	1686	98	67
47X-3, 20–22	439.31	454.73	2.51	20.56	0.064	0.42	8.3	0.127	940	48	42
47X-3, 30–32	439.41	454.83	4.65	17.76	0.035	0.58	11.3	0.209	1255	64	332
47X-3, 40–42	439.51	454.93	3.56	19.72	0.035	0.52	9.2	0.160	1382	55	95
47X-3, 50–52	439.61	455.03	2.83	20.64	0.036	0.35	7.8	0.122	916	46	27
47X-3, 61–63	439.72	455.14	2.71	20.98	0.029	0.24	8.1	0.113	765	48	26
47X-3, 70–72	439.81	455.23	4.70	19.58	0.034	0.68	12.4	0.224	1319	107	51
47X-3, 80–82	439.91	455.33	4.86	17.33	0.032	0.64	12.4	0.225	1327	67	38
47X-3, 90–92	440.01	455.43	3.14	20.08	0.026	0.46	8.7	0.133	977	72	48
47X-3, 100–102	440.11	455.53	2.97	20.64	0.036	0.41	8.3	0.120	854	57	32
47X-3, 110–112	440.21	455.63	2.56	20.77	0.028	0.39	7.6	0.119	746	45	27

Table 3 (continued).

Core, section, interval (cm)	Depth (mbsf)	Depth (mcd)	Al (%)	Ca (%)	P (%)	K (%)	Si (%)	Ti (%)	Ba (ppm)	V (ppm)	Cu (ppm)
47X-3, 120–122	440.31	455.73	2.41	21.41	0.026	0.39	7.1	0.111	698	46	26
47X-3, 130–132	440.41	455.83	2.63	21.05	0.012	0.33	7.4	0.113	837	52	56
47X-3, 140–142	440.51	455.93	2.96	20.75	0.032	0.27	8.3	0.119	879	61	41
47X-4, 0–2	440.61	456.03	3.40	23.87	0.032	0.45	9.8	0.145	1079	55	47
47X–4, 10–12	440.71	456.13	3.11	22.18	0.027	0.39	9.1	0.133	957	57	31
47X–4, 20–22	440.81	456.23	3.91	22.71	0.032	0.51	10.8	0.162	1067	52	69
47X–4, 30–32	440.91	456.33	3.90	20.82	0.037	0.59	10.6	0.169	1049	57	60
47X–4, 40–42	441.01	456.43	3.53	21.25	0.040	0.47	9.8	0.155	1259	66	41
47X-4, 50–52	441.11	456.53	1.89	26.72	0.051	0.38	7.0	0.081	1117	39	25
47X-4, 60–62	441.21	456.63	1.45	27.64	0.043	0.20	6.1	0.066	1006	49	34
47X–4, 70–72	441.31	456.73	1.74	26.56	0.026	0.21	6.1	0.076	801	28	29
47X-4, 80–82	441.41	456.83	1.95	24.37	0.027	0.29	6.3	0.085	610	47	24
47X-4, 90–92	441.51	456.93	2.54	23.09	0.030	0.37	7.5	0.117	764	69	52
47X-4, 100–102	441.61	457.03	5.77	14.51	0.027	0.74	14.7	0.280	1377	53	59
47X-4, 110–112	441.71	457.13	5.15	19.70	0.042	0.73	13.0	0.262	1360	86	59
47X-4, 120–122	441.81	457.23	3.56	22.30	0.064	0.54	9.6	0.147	1031	56	37
47X-4, 130–132	441.91	457.33	3.93	21.83	0.064	0.52	10.1	0.167	1127	47	24
47X-4, 140–142	442.01	457.43	4.40	22.04	0.057	0.55	11.9	0.207	1575	63	70
47X-5, 0–2	442.11	457.53	1.98	21.98	0.044	0.25	7.5	0.092	1153	36	40
47X-5, 10–12	442.21	457.63	2.49	23.57	0.031	0.32	7.3	0.115	908	41	62
47X-5, 20–22	442.31	457.73	3.81	20.26	0.030	0.51	10.1	0.172	1072	31	48
47X-5, 30–32	442.41	457.83	4.85	16.05	0.020	0.75	13.6	0.253	1242	48	46
47X-5, 40–42	442.51	457.93	4.94	18.59	0.047	0.77	13.6	0.213	1424	88	49
47X-5, 50–52	442.61	458.03	5.07	18.02	0.056	0.75	13.7	0.220	1321	76	39
47X-5, 60–62	442.71	458.13	3.56	21.90	0.069	0.57	10.7	0.152	1408	68	40
47X–5, 70–72	442.81	458.23	2.25	24.68	0.064	0.38	7.9	0.097	1185	57	28
47X-5, 80–82	442.91	458.33	2.47	22.71	0.043	0.32	7.9	0.121	1228	54	60
47X-5, 90–92	443.01	458.43	2.92	22.04	0.034	0.37	9.0	0.133	1132	50	63
47X-5, 100–102	443.11	458.53	4.12	19.23	0.031	0.58	12.1	0.203	1352	59	73
47X-5, 110–112	443.21	458.63	6.50	11.97	0.037	0.94	18.8	0.374	1411	91	39
47X-5, 120–122	443.31	458.73	4.53	19.14	0.028	0.59	12.4	0.206	1462	30	53
47X-5, 130–132	443.41	458.83	3.61	20.08	0.054	0.47	10.5	0.161	1404	35	54
47X-5, 140–142	443.51	458.93	4.49	18.44	0.053	0.61	12.8	0.201	1780	36	41
47X-6, 0–2	443.61	459.03	3.73	17.76	0.036	0.52	10.6	0.163	1301	99	74
47X-6, 10–12	443.71	459.13	4.33	19.48	0.039	0.51	11.6	0.188	1164	74	29
47X-6, 20–22	443.81	459.23	2.99	20.05	0.025	0.43	8.4	0.153	1082	143	44
47X-6, 30–32	443.91	459.33	3.46	22.09	0.036	0.44	10.9	0.170	1412	45	43
47X-6, 40–42	444.01	459.43	2.01	21.30	0.031	0.27	6.9	0.092	985	36	67
47X-6, 50–52	444.11	459.53	2.01	24.67	0.035	0.25	8.0	0.090	1100	55	23
47X-6, 60–62	444.21	459.63	2.58	20.67	0.031	0.32	8.1	0.116	1078	36	45
47X-6, 70–72	444.31	459.73	2.54	20.24	0.029	0.37	8.4	0.110	1001	55	36
47X-6, 80–82	444.41	459.83	3.40	22.35	0.037	0.46	10.5	0.141	1242	79	22
47X-6, 90–92	444.51	459.93	3.93	19.65	0.034	0.50	11.3	0.170	1423	48	38
47X-6, 100–102	444.61	460.03	4.26	21.56	0.035	0.47	11.7	0.191	1465	57	130
47X-6, 110–112	444.71	460.13	2.69	20.45	0.031	0.36	8.0	0.127	1178	50	31
47X-6, 120–122	444.81	460.23	2.03	25.14	0.047	0.27	7.7	0.090	1400	71	55
47X-6, 130–132	444.91	460.33	2.21	21.25	0.034	0.27	7.3	0.103	1190	53	34
47X-6, 140–142	445.01	460.43	2.61	20.15	0.034	0.34	8.5	0.127	807	93	46
47X-7, 0–2	445.11	460.53	4.53	15.01	0.022	0.65	12.4	0.233	1020	50	43
47X-7, 10–12	445.21	460.63	4.92	15.12	0.018	0.73	13.6	0.278	1265	163	60
47X-7, 20–22	445.31	460.73	3.91	17.84	0.023	0.46	10.8	0.213	919	231	34
47X-7, 30–32	445.41	460.83	3.11	20.21	0.035	0.36	8.8	0.138	1041	45	49
47X-CC, 0–2	445.51	460.93	2.20	24.12	0.042	0.28	7.3	0.100	996	53	18
47X-CC, 10–12	445.61	461.03	2.13	23.33	0.035	0.31	7.3	0.090	886	58	18
47X-CC, 20–22	445.71	461.13	2.72	22.26	0.034	0.39	8.4	0.115	1078	66	34
47X-CC, 30–32	445.81	461.23	4.01	19.78	0.032	0.51	10.9	0.170	1171	68	52

Note: Major elements (Al, Ca, P, K, Si, and Ti) reported as percentage elemental (not oxide) concentrations and minor elements (Ba, V, and Cu) reported in ppm.

ratios. Silica concentrations are not especially elevated at these times of supposed high productivity when compared to the values for the Holocene Amazon Fan samples.

The average K/Al value of the latest Miocene samples is considerably higher than that from the older material, but similar to the Holocene fan sediment. This probably indicates an increased proportion of illite in the siliciclastic fraction in the late Miocene. Similarly, average Ti/Al values are highest in the same sample run and again match the Holocene results. This may result from the change in clay mineralogy inferred from K/Al data and/or an increased proportion of heavy minerals in the clastic fraction of the sediments. For both elements, these long-term changes in average values are simply explained by the growth of the Amazon Fan in the late Miocene (Castro et al., 1978). This corresponded to a time when the clay minerals of Ceara Rise sediments switched from predominantly kaolinite to illite and the mass accumulation rate of non-carbonate material increased substantially (Curry, Shackleton, Richter, et al., 1995).

Short-Term Changes in Elemental Ratios

Each run of samples collected at 10-cm intervals allows investigation of the variations in elemental ratios, representing changing sediment composition, over periods of tens of thousands of years. Correlation coefficients between Ba/Al and other ratios are cited in the captions to the figures, which show the stratigraphic positions of the ratios. Where sufficient analyses are available, the data have been subjected to spectral analysis based on the Discrete Fourier Transform (methodology in Weedon et al., this volume).

Latest Miocene

In Core 154-926B-17H, pronounced variations in carbonate content suggested by Ca/Al values (Figs. 3, 5A) are also recorded by variations in %550 nm light reflectance and magnetic susceptibility and relate to regular orbital-climatic forcing (Curry, Shackleton, Richter, et al., 1995). Barium ratios are so similar to the Holocene values that a predominantly detrital source is likely (Fig. 5A). However, there is a moderate correlation with inferred carbonate contents (Fig. 5A), suggesting that a small productivity signal is superimposed on the detrital background. It is possible that these Ba/Al values were lowered by dissolution of barites during diagenetic sulfate reduction. The average Si/Al and P/Al values are also similar to the Holocene siliciclastics ratios. However, these ratios are weakly correlated with Ba/Al, so a small productivity signal is indicated.

Table 4. Correlation matrix of elemental concentrations excluding the three Amazon Fan samples (n = 494).

	Ca	P	K	Si	Ti	Ba
Al	–0.444	+0.275	**+0.759**	**+0.905**	**+0.953**	–0.238
Ca		–0.071	–0.324	–0.430	–0.449	+0.085
P			+0.141	+0.306	+0.186	+0.113
K				**+0.632**	**+0.751**	**–0.500**
Si					**+0.859**	+0.110
Ti						–0.265

Note: Cu and V are ommitted as their concentrations are below the limit of quantitation for all samples. Underlined values = the probability that there is no correlation is less than 0.0001. Bold values = P<0.0001 and r is greater than 0.5.

K/Al and Ti/Al are similar to Holocene values and, though varying erratically, they show some covariation. This similar behavior might indicate short-term, irregular variations in clay mineralogy and/or variations in heavy mineral proportions.

Middle Miocene

Ca/Al results from Core 154-926A-26H (Fig. 5B) show that although inferred carbonate variations are pronounced, Ba/Al is very similar to Holocene values and varies erratically. Si/Al values are less than the Holocene Amazon Fan results and weakly correlated with Ba/Al. P/Al values are similar to today and there is no correlation with Ba/Al. Therefore, there is no evidence for short-term productivity variations. K/Al and Ti/Al are low and essentially constant, suggesting less illite and/or heavy minerals compared to the late Miocene to Holocene sediments.

Oligocene/Miocene Boundary

In Cores 154-926B-50X and 51X the average Ba/Al values are greater than the Holocene siliciclastic values, suggesting higher average productivity than today (Fig. 6). Biogenic silica was not identified in these cores on board, but small quantities of diatoms, radiolaria, silicoflagellates, and sponge spicules were recorded from the overlying core. Pore-water SiO_2 is distinctly elevated at this level in Hole 926B, suggesting that Si/Al values have been lowered due to silica dissolution (Curry, Shackleton, Richter, et al., 1995). The weak, although significant, correlation of Ba/Al with Si/Al and P/Al (Fig. 6), suggests that all three relate to productivity variations. Maximum productivity apparently occurred during maximum burial/preservation of carbonate. Spectral analysis reveals regular 1-m variations in all these parameters as well carbonate contents from Ca/Al (Fig. 7). The cyclicity corresponds to indirect control by the 40,000-yr (obliquity) orbital-climatic cycles (Weedon et al., this volume). K/Al and Ti/Al show the same patterns as found in the middle Miocene.

Mid-Oligocene

Two data sets have been generated for mid-Oligocene strata, although the time intervals represented are slightly different (Table 1). In Core 154-926B-64X, Ca/Al and hence carbonate contents vary regularly with a wavelength of about 1 m, which is indicative of 40,000-yr cyclicity (Figs 8, 9; Weedon et al., this volume). Ba/Al, Si/Al, and P/Al mostly exceed Holocene values and show strongly correlated, regular cyclicity (Fig. 8). No biosiliceous material has been described from the core, but high pore-water silica implies dissolution of biogenic material. Again, increased productivity with maxima coincident with maximum carbonate burial/preservation is indicated. K/Al and Ti/Al show values similar to results from the middle Miocene and Oligocene/Miocene boundary.

The same patterns as seen in Core 154-926B-64X are also observed in Core 154-929A-47X (Fig. 10). However, while variations in Ba/Al are strongly correlated with Si/Al and P/Al, regular cyclicity cannot be demonstrated rigorously for Si/Al (Fig. 11). Nevertheless, pore-water silica concentrations are high, and radiolaria and diatoms form a significant portion of the underlying core. Average Si/Al values are also much higher than any other intervals examined. Thus, regularly varying high productivity is indicated for this deep-water site. Aside from a small interval of relatively high K/Al at the top of the core, K/Al and Ti/Al values are again near-constant and lower than the late Miocene results.

Table 5. Carbonate determinations for Core 154-926B-17H.

Section	Interval (cm)	$CaCO_3$ (%)
2	54–56	80.0
	64–56	75.4
	74–76	58.4
	84–86	54.4
	94–96	55.5
	104–106	72.6
	114–116	69.2
	124–126	62.1
	134–136	53.6
	144–146	65.1
3	4–6	73.7
	14–16	72.1
	24–26	65.0
	34–36	53.9
	44–46	54.0
	54–56	61.4
	64–66	68.3
	74–76	71.0
	84–86	71.5
	94–96	73.2
	104–116	69.2
	114–116	63.1
	124–126	73.3
	134–136	78.5
	144–146	73.3
4	4–6	54.0
	14–16	67.7
	24–26	76.6
	34–36	71.2
	44–46	51.1
	54–56	44.3
	64–66	46.7
	74–76	61.9
	84–86	61.7
	94–96	56.0
	104–106	51.0
	113–115	70.5

SUMMARY AND CONCLUSIONS

Despite the potential problems connected with the interpretation of elemental ratios in terms of the controlling factors and mineralogy, a clear pattern emerges from the results. As demonstrated during Leg 154, illite concentrations in the clastic fraction, as indicated by K/Al, were low from the mid-Oligocene to the middle Miocene. Increased illite proportions in the clastic fraction occurred in the latest Miocene. The similar behavior of K/Al and Ti/Al over tens of millions of years, as well as covariation in the late Miocene, might relate to changing clay mineralogy and/or heavy mineral proportions. These changes were probably associated with the growth of the Amazon Fan and an increased flux of siliciclastic material towards the Ceara Rise. This probably coincided with the demise of the South American seaways (Rasanen et al., 1995). If the long-term changes in Ti/Al relate to heavy mineral proportions rather than clay mineralogy, then it might imply a change in sediment provenance that is connected to the derivation of sediment from the Andes rather than more local sources.

Average Ba/Al, Si/Al, and P/Al values suggest much higher average productivity in the late early Oligocene and at the Oligocene/Miocene boundary when compared to today. The short-term correlation of Si/Al with Ba/Al and P/Al in the mid-Oligocene and Oligocene/Miocene boundary shows that the biosiliceous material in the sediment is related to higher productivity and not just preservation. Therefore, the low values of pore-water silica and less common siliceous microfossils in sediments from the early and middle part of the late Oligocene imply that the two periods of increased productivity were separated by a period of lower average productivity. Curry, Shackleton, Richter, et al. (1995), suggested that the changes in deep-water circulation patterns, in both the early Oligocene and latest Oligocene/earliest Miocene, would account for these episodes of increased productivity.

The current data also show that productivity varied on a 40,000-yr time scale in the mid-Oligocene and at the Oligocene/Miocene boundary. Maximum productivity occurred during the peak of carbonate burial and minimum carbonate dissolution. Considering the strength of this 40,000-yr (orbital-obliquity) cycle and the lack of ev-

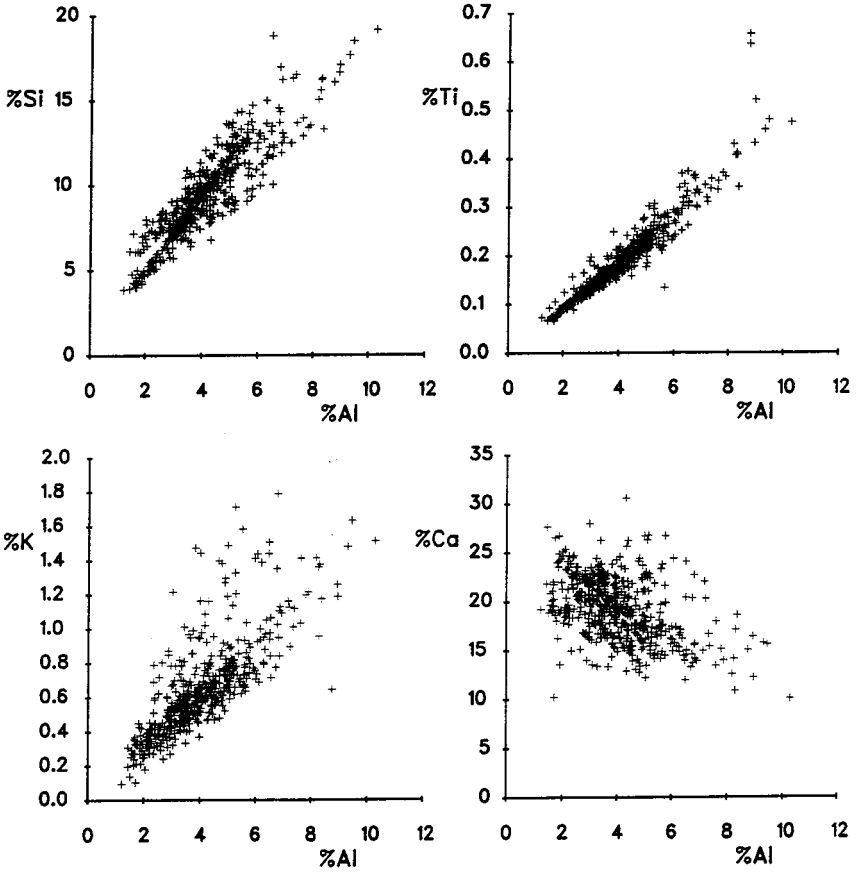

Figure 2. Scatter plots of selected elemental concentrations against aluminum for all the results from the Ceara Rise (N = 494). The strong correlations of Ti, K, and Si with Al (Table 4) indicate that all of these elemental concentrations are related to the proportions of siliciclastic minerals, especially clays. The inverse relationship between Ca and Al partly results from varying proportions of calcium carbonate and clay minerals. However, the scatter around this relationship probably results from the presence of calcium in certain clays.

idence for a 20,000-yr component, the mechanism responsible for these short-term variations must have involved high-latitude climatic processes that affected, for example, bottom-water formation.

ACKNOWLEDGMENTS

Mark Maslin (University College, London) kindly supplied the Leg 155 Amazon Fan samples, and Jan Backman (Stockholm) provided the calcium carbonate determinations. This work was supported by NERC grant GST/02/971. C. Robinson, S. Purdy, and T. Papoloizou (Luton) are thanked for their analytical work. Thanks also to H. Brumsack and M. Delaney for their constructive criticisms.

REFERENCES

Archer, D., Lyle, M., Rodgers, K., and Froelich, P., 1993. What controls opal preservation in tropical deep-sea sediments? *Paleoceanography,* 8:7–21.

Arthur, M.A., Jenkyns, H.C., Brumsack, H., and Schlanger, S.O., 1988. Stratigraphy, geochemistry, and paleo-oceanography of organic carbon-rich Cretaceous sequences. *In* Ginsburg, R.N., and Beaudoin, B. (Eds.), *Cretaceous Resources, Events and Rhythms.* NATO ASI Ser., 304:75–119.

Benjamin, M., Johnson, N.M., and Naeser, C.W., 1987. Recent rapid uplift in the Bolivian Andes: evidence from fission-track dating. *Geology,* 15:680–683.

Brumsack, H.-J., 1986. The inorganic geochemistry of Cretaceous black shales (DSDP Leg 41) in comparison to modern upwelling sediments from the Gulf of California. *In* Summerhayes, C.P., and Shackleton, N.J. (Eds.), *North Atlantic Palaeoceanography.* Geol. Soc. London Spec. Publ., 21:447–462.

Brumsack, H.-J., and Gieskes, J.M., 1983. Interstitial water trace-metal chemistry of laminated sediments from the Gulf of California, Mexico. *Mar. Chem.,* 14:89–106.

Castro, J.C., Miura, K., and Estrela-Braga, J.A.E., 1978. Stratigraphic and structural framework of the Foz do Amazonas Basin. *Proc. Annu. Offshore Technol. Conf.*, 3:1843–1847.

Charles, C.D, Froelich, P.N., Zibello, M.A., Mortlock, R.A., and Morley, J.J., 1991. Biogenic opal in southern ocean sediments over the last 450,000 years: implications for surface water chemistry and circulation. *Paleoceanography,* 6:697–728.

Curry, W., Shackleton, N.J., Richter, C., et al., 1995. *Proc. ODP, Init. Repts.,* 154: College Station, TX (Ocean Drilling Program).

Dymond, J., Suess, E., and Lyle, M., 1992. Barium in deep-sea sediment: a geochemical proxy for paleoproductivity. *Paleoceanography,* 7:163–182.

Filipelli, G.M., and Delaney, M.L., 1994. The oceanic phosphorus cycle and continental weathering during the Neogene. *Paleoceanography,* 9:643–652.

Flood, R.D., Piper, D.J.W., Klaus, A., et al., 1995. *Proc. ODP, Init. Repts.,* 155: College Station, TX (Ocean Drilling Program).

Gingele, F., and Dahmke, A., 1994. Discrete barium particles and barium as tracers of paleoproductivity in South Atlantic sediments. *Paleoceanography,* 9:151–168.

Haq, B.U., Hardenbol, J., and Vail, P.R., 1987. Chronology of fluctuating sea levels since the Triassic. *Science,* 235:1156–1167.

Lea, D.W., and Spero, H.J., 1994. Assessing the reliability of paleochemical tracers: barium uptake in the shells of planktonic foraminifera. *Paleoceanography,* 9:445–452.

Lyle, M.D., Murray, D.M., Finney, B.P., Dymond, J., Robinson, J.M., and Brookforce, K., 1988. The record of late Pleistocene biogenic sedimentation in the east tropical Pacific Ocean. *Paleoceanography,* 3:39–59.

Norry, M.J., Dunham, A.C., and Hudson, J.D., 1994. Mineralogy and geochemistry of the Peterborough Member, Oxford Clay Formation, Jurassic, UK: element fractionation during mudrock sedimentation. *J. Geol. Soc.,* 151:195–207.

Rasanen, M.E., Linna, A.M., Santo, J.C.R., and Negri, F.R., 1995. Late Miocene tidal deposits in the Amazonian Foreland Basin. *Science,* 269:386–389.

Schmitz, B., 1989. The TiO_2/Al_2O_3 ratio in the Cenozoic Bengal Abyssal Fan sediments and its use as a paleostream energy indicator. *Mar. Geol.,* 76:195–206.

Shimmield, G.B., and Mowbray, S.R., 1991. The inorganic geochemical record of the northwest Arabian Sea: a history of productivity variation over the last 400 k.y. from Sites 722 and 724. *In* Prell, W.L., Niitsuma, N., et al., *Proc. ODP, Sci. Results*, 117: College Station, TX (Ocean Drilling Program), 409–429.

Smith, A.G., Smith, D.G., and Funnell, B.M., 1994. *Atlas of Mesozoic and Cenozoic Coastlines:* Cambridge (Cambridge Univ. Press).

Van Buchem, F.S.P., McCave, I.N., and Weedon, G.P., 1994. Orbitally induced small-scale cyclicity in a siliciclastic epicontinental setting (Lower Lias, Yorkshire, UK). *In* de Boer, P.L., and Smith, D.G., *Orbital Forcing and Cyclic Sequences.* Int. Assoc. Sedimentol. Spec. Publ., 19:345–366.

Van Cappellen, P., and Ingall, E.D., 1994. Benthic phosphorus regeneration, net primary production, and ocean anoxia: a model of the coupled marine biogeochemical cycles of carbon and phosphorus. *Paleoceanography*, 9:677–692.

Webb, S.D., 1995. Biological implications of the Middle Miocene Amazon seaway. *Science*, 269:361–362.

Weedon, G.P., and Shimmield, G.B., 1991. Late Pleistocene upwelling and productivity variations in the Northwest Indian Ocean deduced from spectral analyses of geochemical data from Sites 722 and 724. *In* Prell, W.L., Niitsuma, N., et al., *Proc. ODP, Sci. Results*, 117: College Station, TX (Ocean Drilling Program), 431–443.

Date of initial receipt: 11 December 1995
Date of acceptance: 14 May 1996
Ms 154SR-129

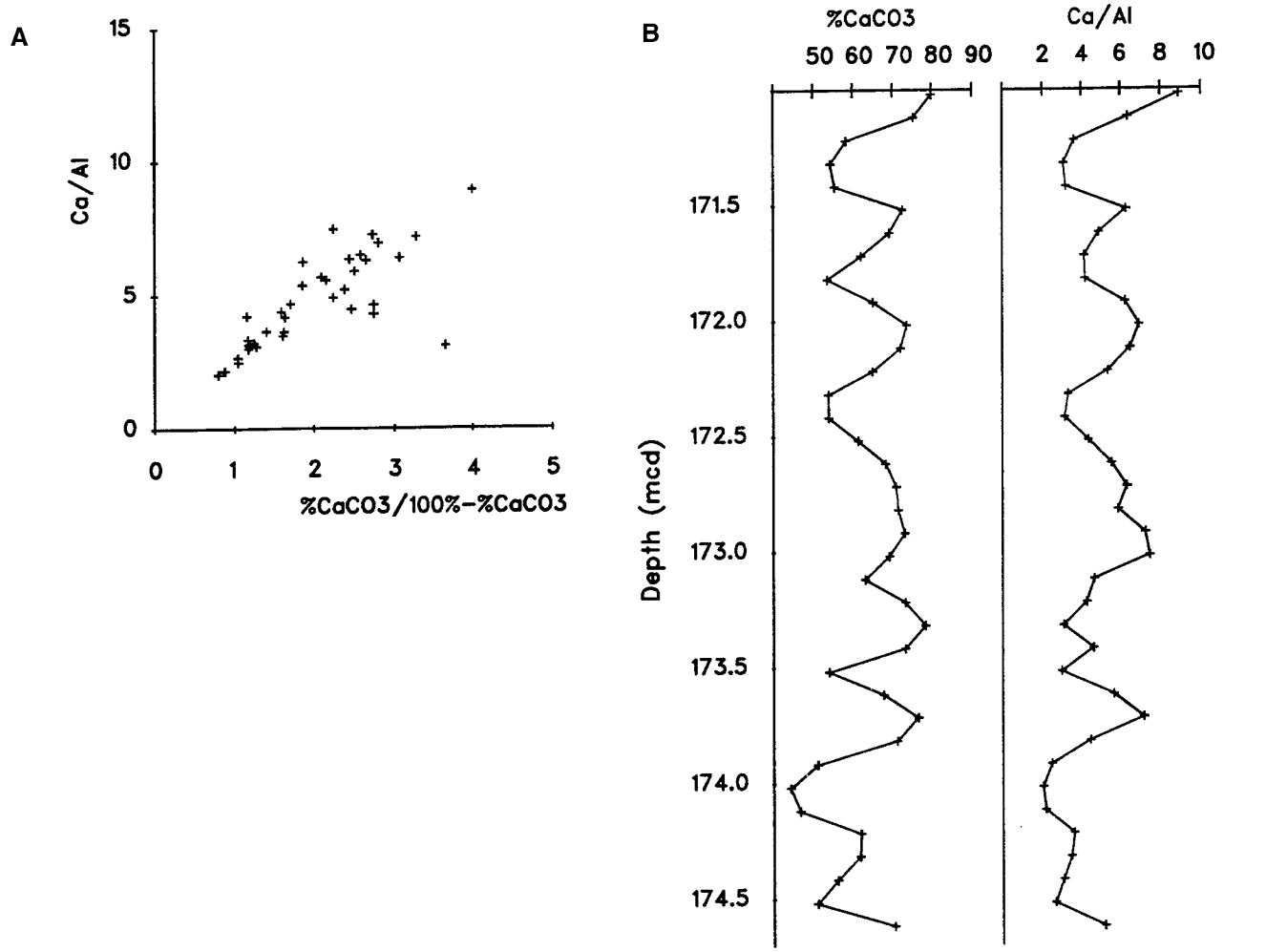

Figure 3. **A.** Carbonate/non-carbonate vs. Ca/Al values follow an approximately linear relationship in Core 154-926B-17H, as would be expected if most Ca resides in calcite and Al in clay minerals. **B.** Plotted stratigraphically, the Ca/Al values vary in a similar manner to the measured values of $CaCO_3$ in this core, suggesting that the ratio can be used as a crude proxy for carbonate contents in short stratigraphic intervals.

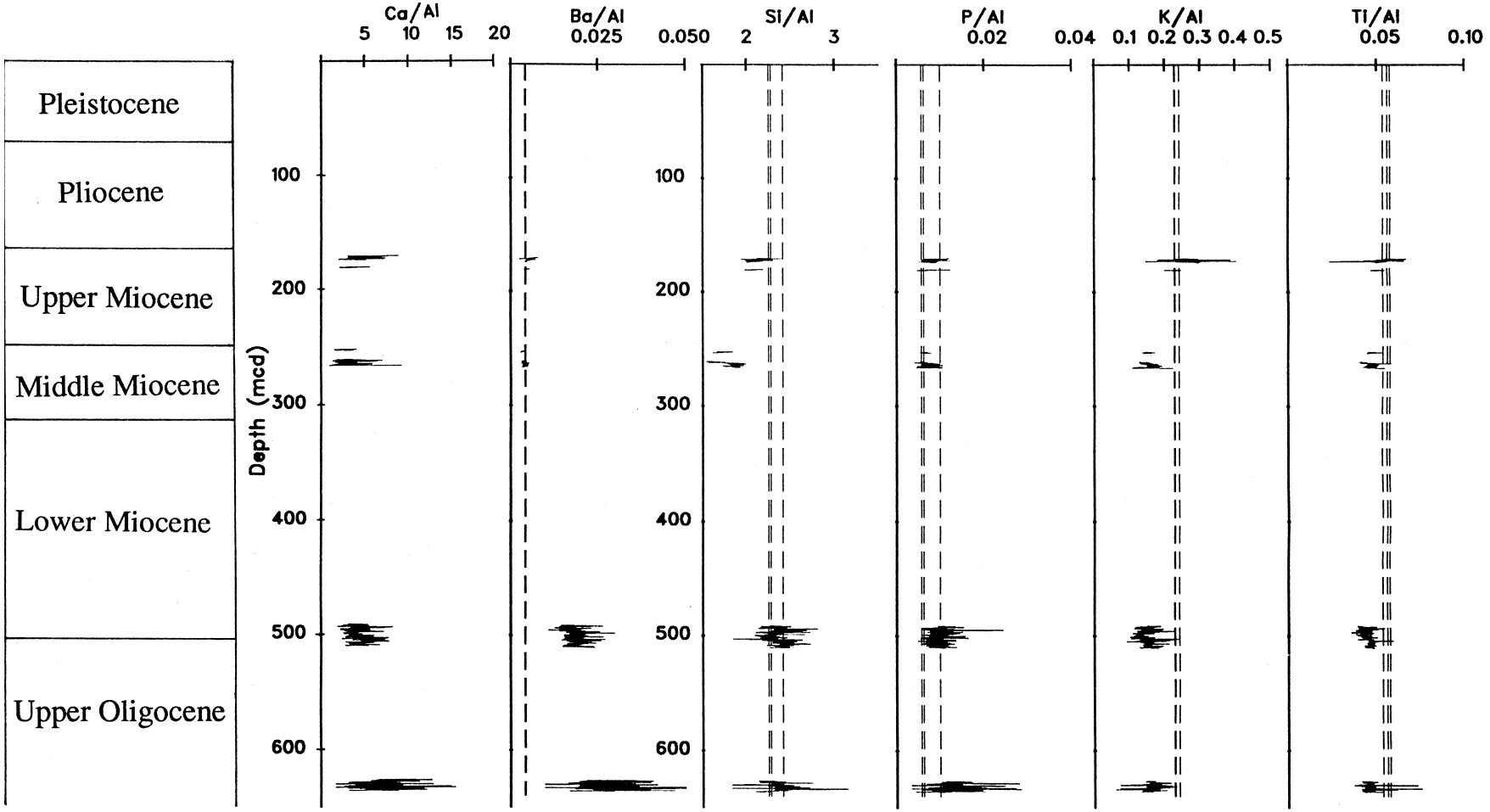

Figure 4. Plot of all the elemental ratios generated for Site 926 (Table 1). Results for Holocene Amazon Fan hemipelagic silty clay from Site 942 (Flood, Piper, Klaus, et al., 1995) are shown as a vertical dashed line. Relatively high K/Al in the Holocene and latest Miocene samples suggest relatively elevated illite proportions in the clay fraction. Higher average Ba/Al, Si/Al, and P/Al at the Oligocene/Miocene boundary and the mid-Oligocene indicate enhanced productivity compared to the Holocene. Note that Ba/Al values for the uppermost and middle Miocene are very close to the values from the Amazon Fan samples.

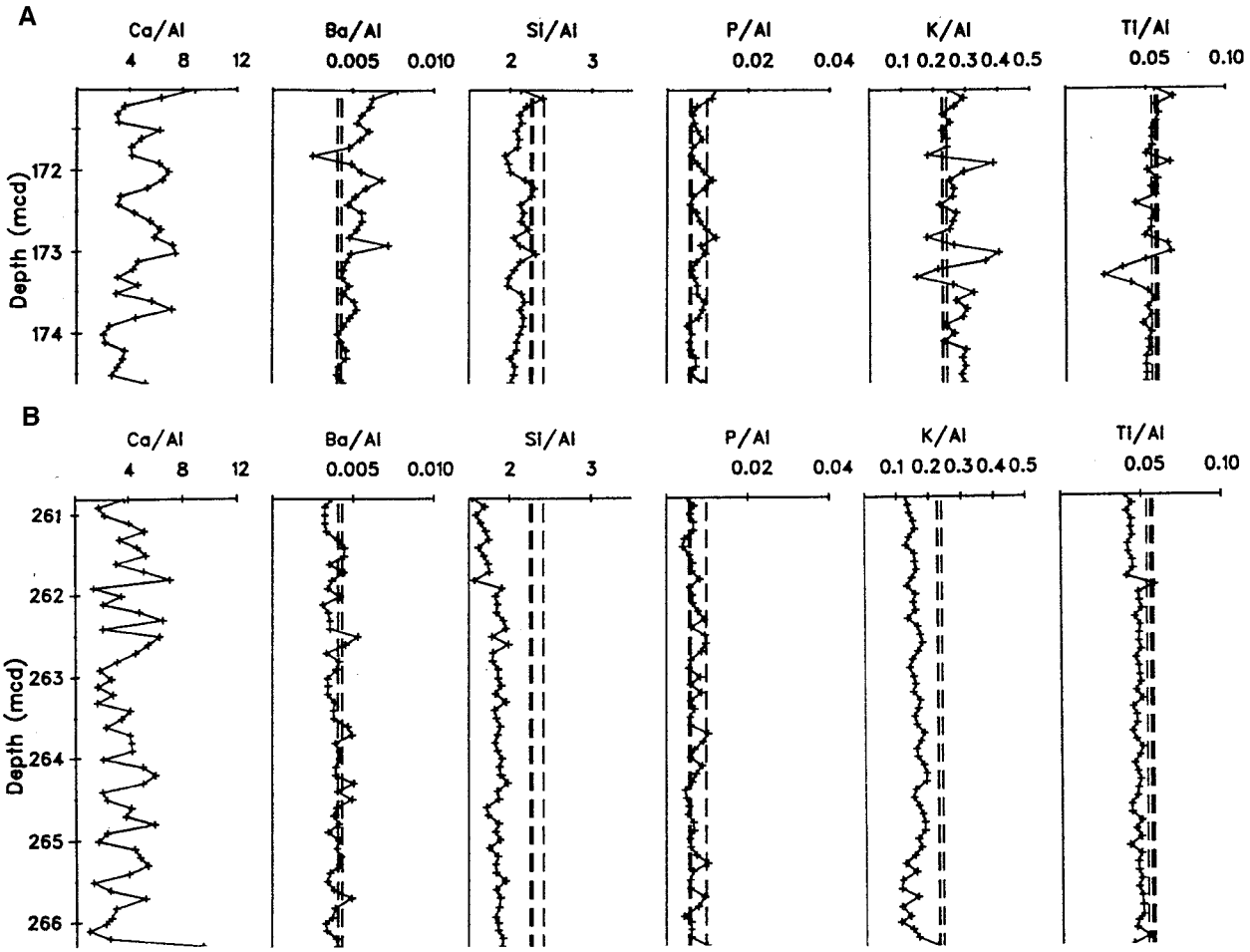

Figure 5. Elemental ratios from sediments deposited (**A**) in the latest Miocene (Core 154-926B-17H) and (**B**) in the middle Miocene (Core 154-926A-26H). Results from the Holocene Amazon Fan samples are shown as dashed lines for comparison. For the latest Miocene samples, Ba/Al is weakly correlated with Ca/Al ($N = 37$, $r = 0.63$, $P < 0.001$), P/Al ($r = 0.59$, $P < 0.001$), and Si/Al ($r = 0.45$, $P < 0.01$). For the middle Miocene samples, Ba/Al is weakly correlated with Ca/Al ($N = 56$, $r = 0.35$, $P < 0.001$) and Si/Al ($r = 0.51$, $P < 0.0001$), but not P/Al ($r = 0.16$, not significant).

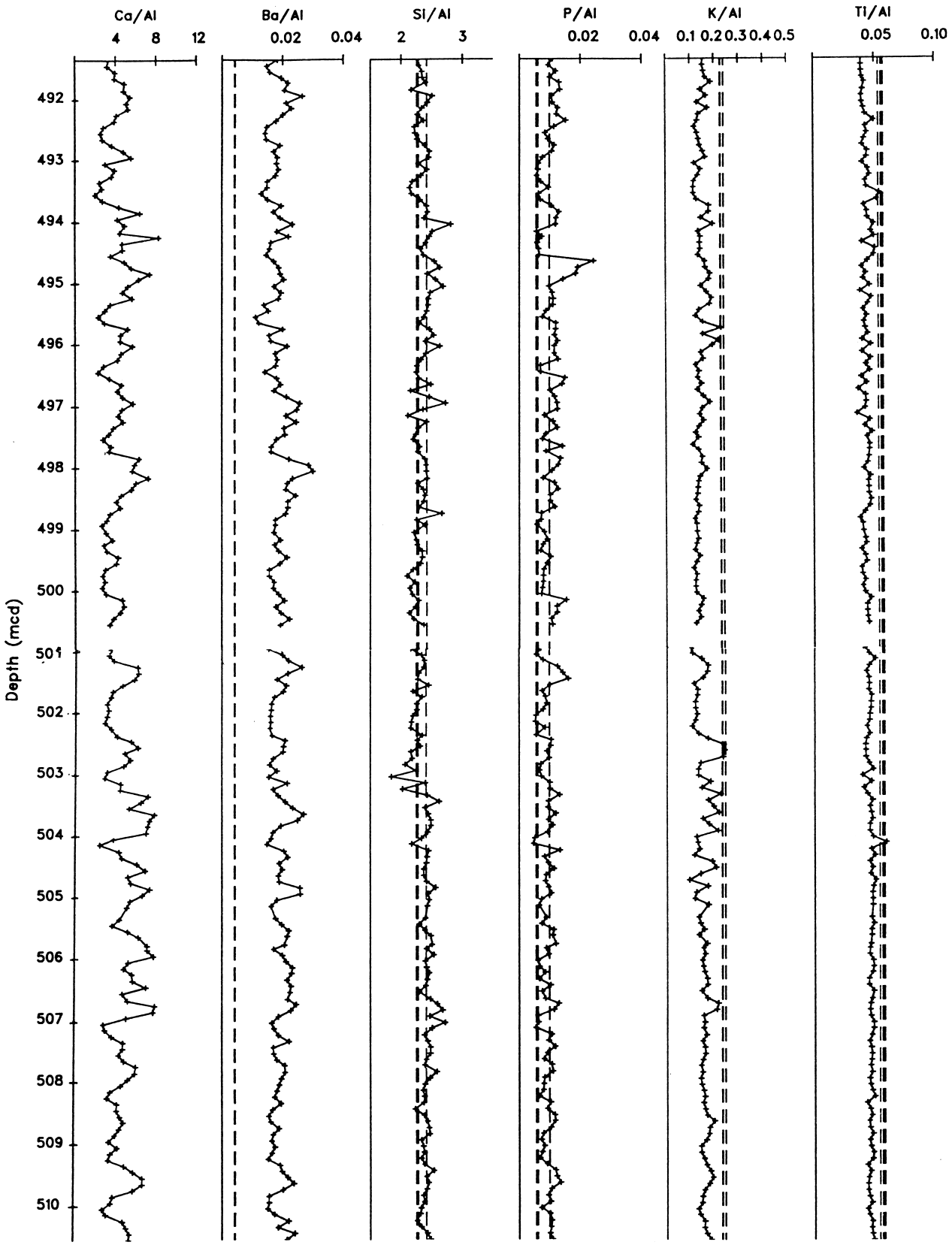

Figure 6. Elemental ratios from samples covering the Oligocene/Miocene boundary from Cores 154-926B-50X and 51X. Ba/Al is moderately correlated with Ca/Al (N = 189, r = 0.63, P < 0.0001), but weakly correlated with P/Al (r = 0.29, P < 0.0001) and Si/Al (r = 0.38, P < 0.0001). The correlations suggest short-term variations in productivity occurred at the Oligocene/Miocene boundary over the Ceara Rise.

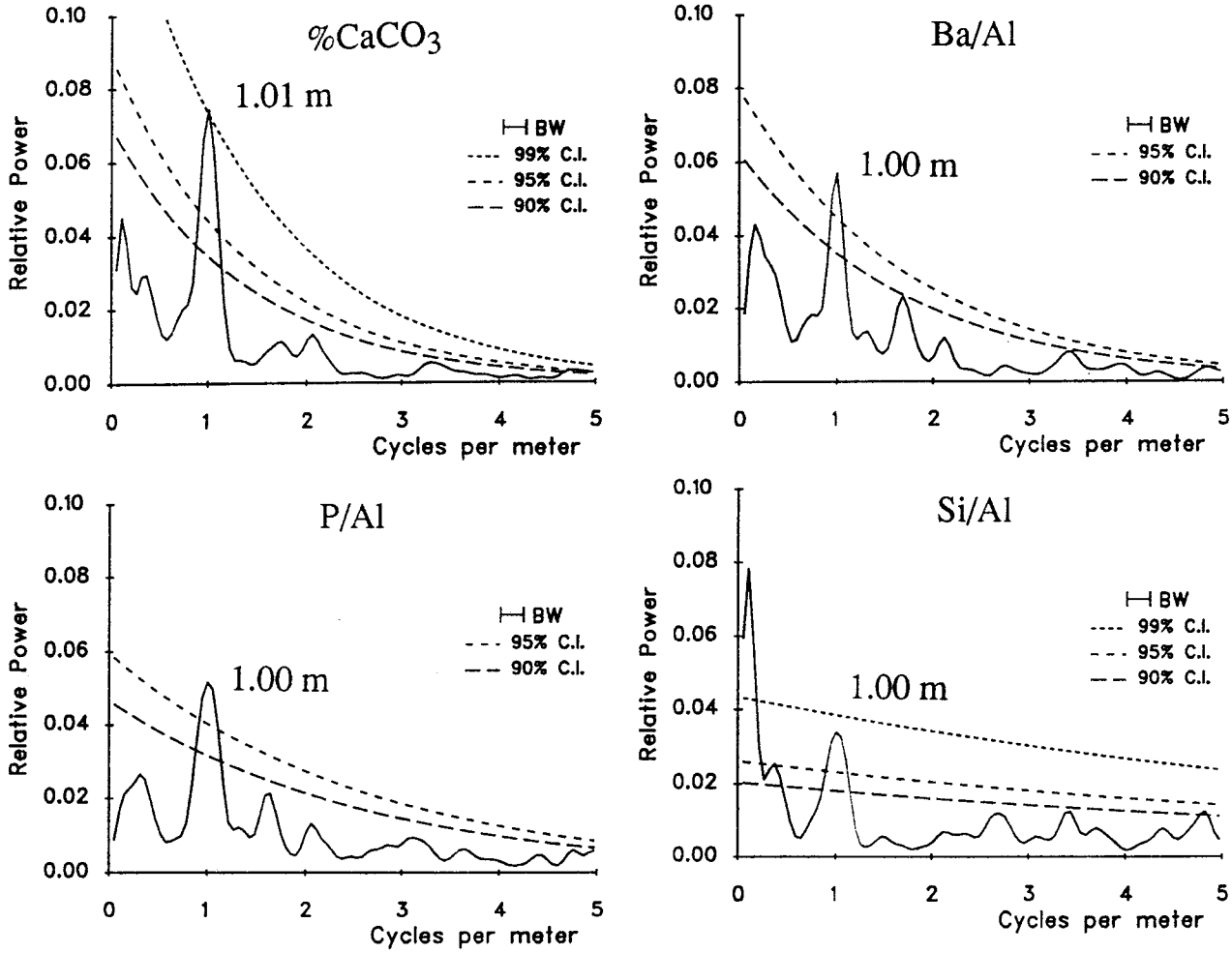

Figure 7. Spectral analysis of certain elemental ratios from the Oligocene/Miocene boundary in Cores 154-926B-50X and 51X. The statistically significant spectral peaks correspond to regular cycles with wavelengths of about 1 m. The cyclicity in Ba/Al, Si/Al, and P/Al results from indirect 40,000-yr orbital-climatic forcing (Weedon et al., this volume).

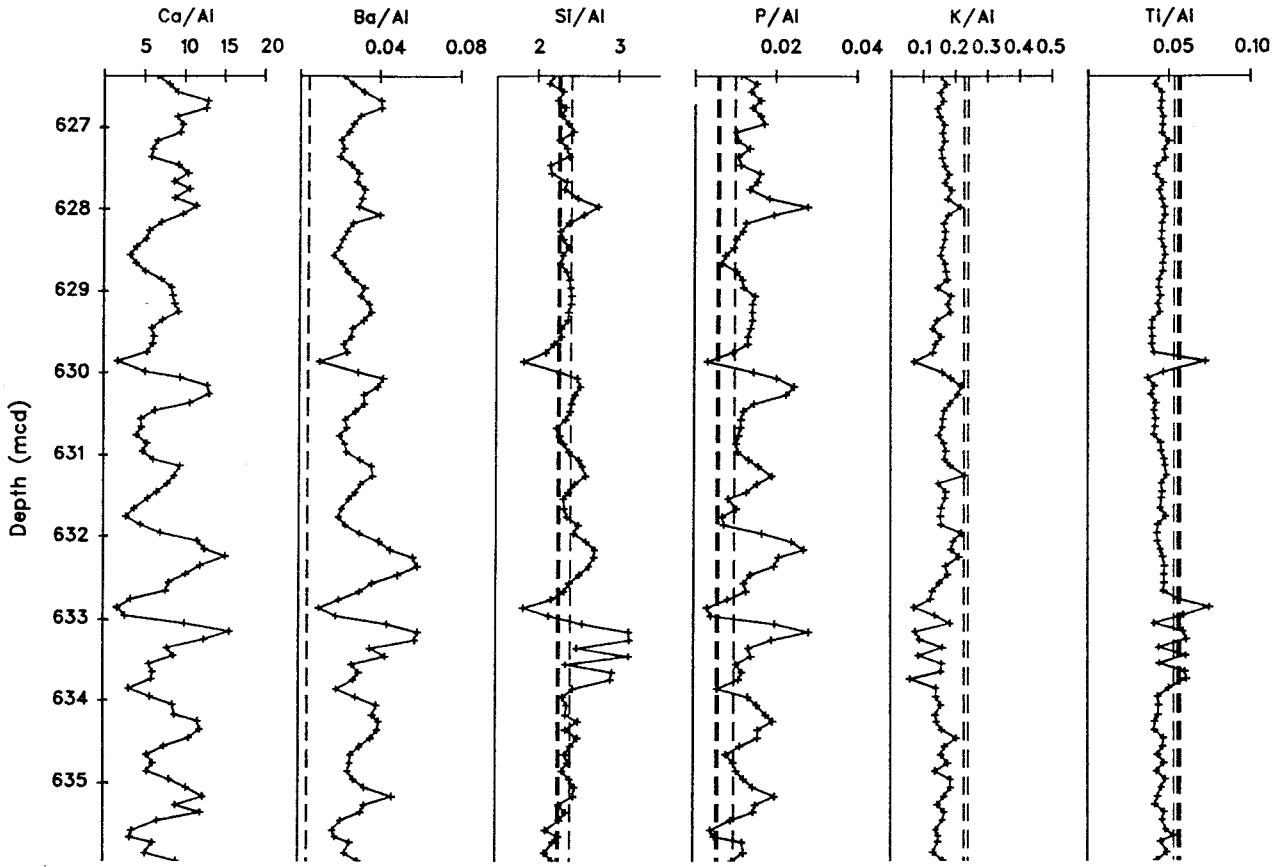

Figure 8. Mid-Oligocene elemental ratios from Core 154-926B-64X. Ba/Al is strongly correlated with Ca/Al (N = 97, r = 0.85), P/Al (r = 0.78), and Si/Al (r = 0.67; P < 0.0001 for all correlations). These correlations suggest strong productivity variations.

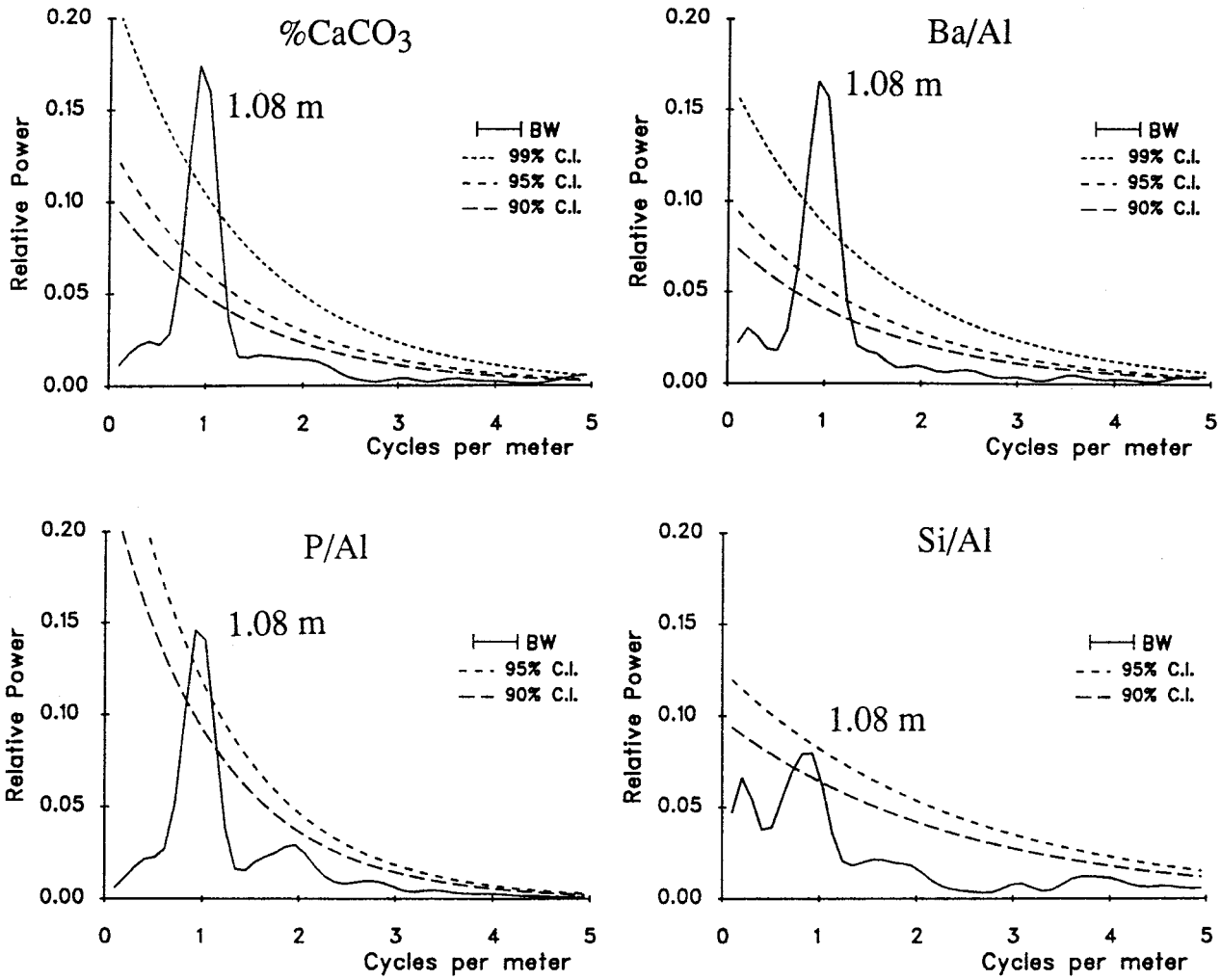

Figure 9. Spectral analysis of mid-Oligocene elemental ratios from Core 154-926B-64X. Regular 40,000-yr cyclicity in productivity is implied by the significant spectral peaks.

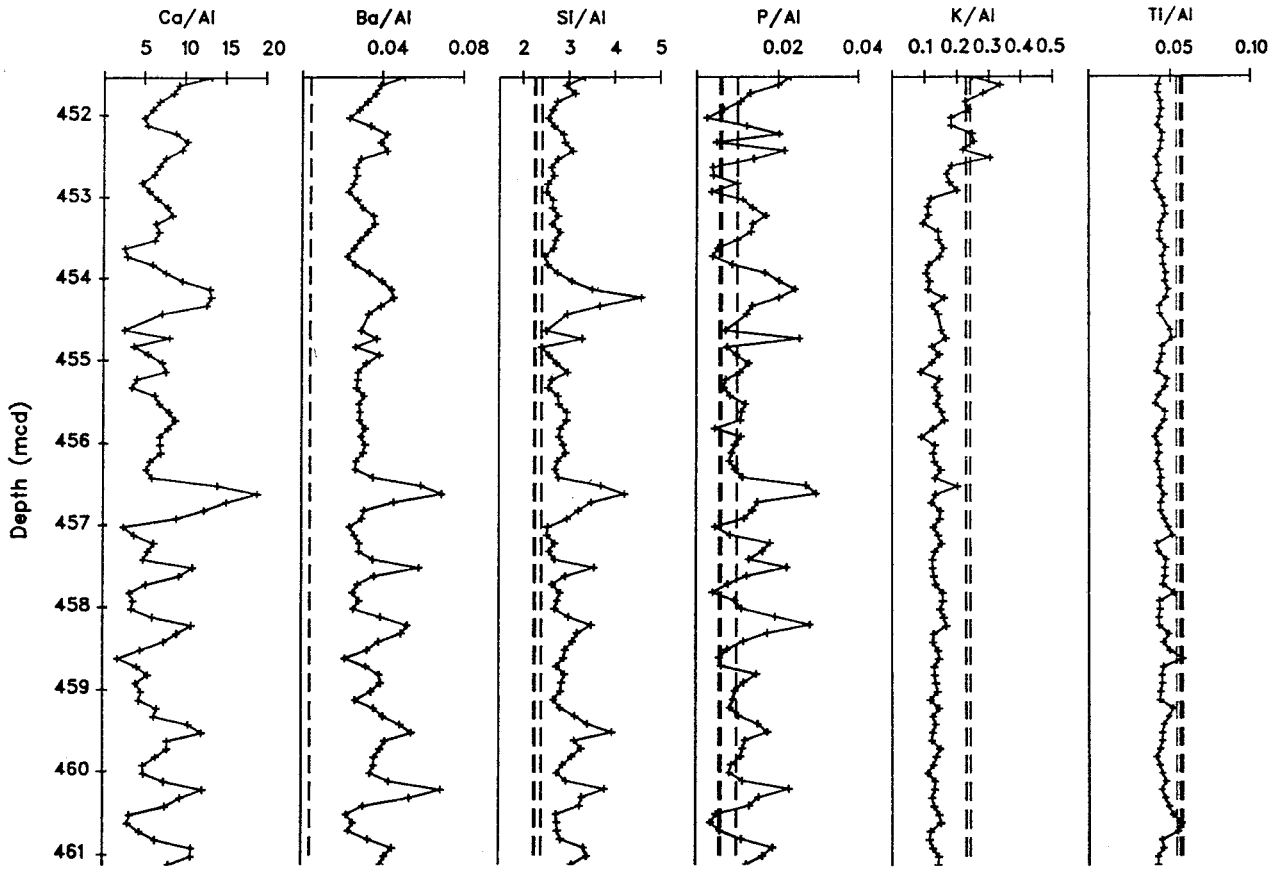

Figure 10. Mid-Oligocene elemental ratios from Core 154-929A-47X. Site 929 is about 60 km from Site 926 (Fig. 1). There is a strong correlation between Ba/Al and Ca/Al (N = 97, r = 0.79), P/Al (r = 0.79), and Si/Al (r = 0.81; P < 0.0001 for all correlations). These results imply strong productivity variations. Average Si/Al values are especially high in this core when compared to the other cores examined, which suggests significantly higher productivity than the Holocene.

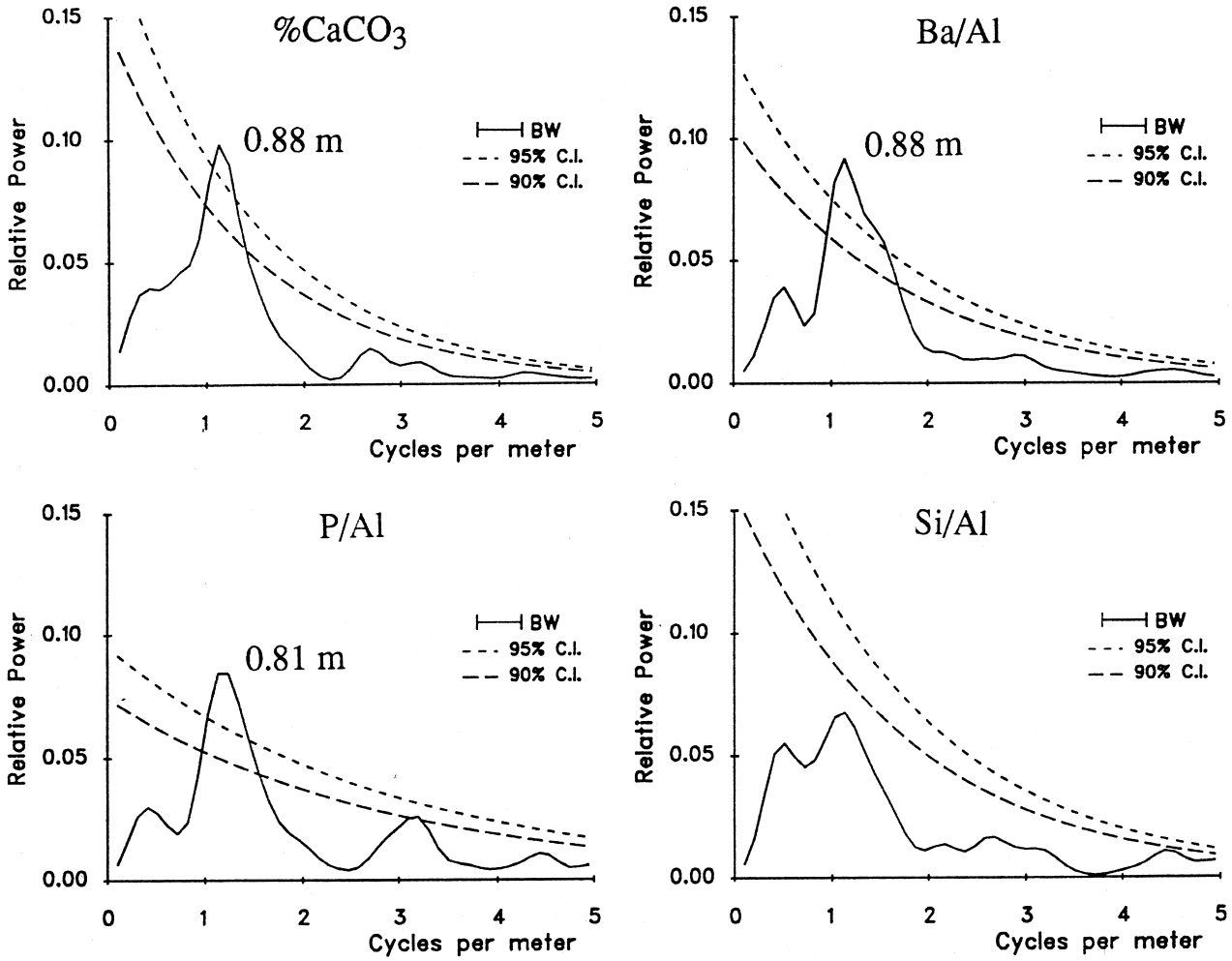

Figure 11. Spectral analysis of mid-Oligocene elemental ratios from Core 154-926B-47X. The spectral peaks indicate regular, approximately 90-cm cyclicity inferred to relate to 40,000-yr cycles in productivity.

Previous Chapter Table of Contents Next Chapter